PLOS BIOLOGY

RESEARCH ARTICLE

Chemokine signaling links cell-cycle progression and cilia formation for left–right symmetry breaking

Jingwen Liu[1‡], Chengke Zhu[2‡], Guozhu Ning[3], Liping Yang[3], Yu Cao[3], Sizhou Huang[4]*, Qiang Wang[3,5]*

1 School of Life Sciences, University of Science and Technology of China, Hefei, China, **2** Key Laboratory of Freshwater Fish Reproduction and Development, Ministry of Education, Key Laboratory of Aquatics Science of Chongqing, College of Animal Science in Rongchang Campus, Southwest University, Chongqing, China, **3** State Key Laboratory of Membrane Biology, Institute of Zoology, University of Chinese Academy of Sciences, Chinese Academy of Sciences, Beijing, China, **4** Development and Regeneration Key Laboratory of Sichuan Province, Department of Anatomy and Histology and Embryology, Chengdu Medical College, Chengdu, China, **5** Institute for Stem Cell and Regeneration, Chinese Academy of Sciences, Beijing, China

‡ These authors share first authorship on this work.
* huangyuy1027@cmc.edu.cn (SH); qiangwang@ioz.ac.cn (QW)

OPEN ACCESS

Citation: Liu J, Zhu C, Ning G, Yang L, Cao Y, Huang S, et al. (2019) Chemokine signaling links cell-cycle progression and cilia formation for left–right symmetry breaking. PLoS Biol 17(8): e3000203. https://doi.org/10.1371/journal.pbio.3000203

Academic Editor: Mary C. Mullins, University of Pennsylvania School of Medicine, UNITED STATES

Received: March 6, 2019

Accepted: August 6, 2019

Published: August 20, 2019

Data Availability Statement: All relevant data are within the paper and its Supporting Information files.

Funding: The research was funded by grants from the National Key Research and Development Program of China (2016YFA0100503, and 2018YFA0800200, QW), the National Natural Science Foundation of China ((31571501, 81921006, and 91739101, QW; 31741091, SZH) and the Strategic Priority Research Program of the Chinese Academy of Sciences (XDA16000000,

Abstract

Zebrafish dorsal forerunner cells (DFCs) undergo vigorous proliferation during epiboly and then exit the cell cycle to generate Kupffer's vesicle (KV), a ciliated organ necessary for establishing left–right (L–R) asymmetry. DFC proliferation defects are often accompanied by impaired cilia elongation in KV, but the functional and molecular interaction between cell-cycle progression and cilia formation remains unknown. Here, we show that chemokine receptor Cxcr4a is required for L–R laterality by controlling DFC proliferation and KV ciliogenesis. Functional analysis revealed that Cxcr4a accelerates G1/S transition in DFCs and stabilizes forkhead box j1a (Foxj1a), a master regulator of motile cilia, by stimulating Cyclin D1 expression through extracellular regulated MAP kinase (ERK) 1/2 signaling. Mechanistically, Cyclin D1–cyclin-dependent kinase (CDK) 4/6 drives G1/S transition during DFC proliferation and phosphorylates Foxj1a, thereby disrupting its association with proteasome 26S subunit, non-ATPase 4b (Psmd4b), a 19S regulatory subunit. This prevents the ubiquitin (Ub)-independent proteasomal degradation of Foxj1a. Our study uncovers a role for Cxcr4 signaling in L–R patterning and provides fundamental insights into the molecular linkage between cell-cycle progression and ciliogenesis.

Introduction

Vertebrates exhibit striking left–right (L–R) asymmetries in the structure and position of their cardiovascular and gastrointestinal systems. Initially, early embryos develop symmetrically along the prospective body midline. This embryonic symmetry is broken during somite stages when an asymmetric fluid flow is generated by motile cilia within the L–R organizer (LRO), a transient structure located at the posterior end of the notochord [1]. Specifically, in zebrafish,

QW). The funders had no role in study design, data collection and analysis, decision to publish, or preparation of the manuscript.

Competing interests: The authors have declared that no competing interests exist.

Abbreviations: 3-MA, 3-methyladenine; aPKC, atypical protein kinase C; ATCC, American Tissue Culture Collection; BrdU, bromodeoxyuridine; caMEK1, constitutively activated version of MEK1; CDK, cyclin-dependent kinase; *cmlc2*, cardiac myosin light chain 2; cMO, control MO; DFC, dorsal forerunner cell; EF1α, eukaryotic translation elongation factor 1α; ERK, extracellular regulated MAP kinase; ES, embryonic stem; FGF, fibroblast growth factor; Foxj1a, forkhead box j1a; FOXM1, forkhead box M1; FOXO1, forkhead box O1; GFP, green fluorescent protein; GSK-3β, glycogen synthase kinase 3β; GST, glutathione S-transferase; HA, hemagglutinin; HEK, human embryonic kidney; *hhex*, hematopoietically expressed homeobox; hpf, hours postfertilization; IgG, immunoglobulin G; KV, Kupffer's vesicle; Lnx2b, ligand of numb-protein X 2b; LPM, left lateral plate mesoderm; L–R, left–right; LRO, L–R organizer; mFoxj1, mouse Foxj1; MGRN1, mahogunin RING finger 1; mKO2, monomeric Kusabira Orange2; MO, morpholino; MZ, maternal zygotic; Nanog, Nanog homeobox; ns, no significant difference; Oct4, Octamer-binding protein 4; Pah1, phosphatidic acid phosphohydrolase 1; p-ERK1/2, phosphorylated ERK1/2; *pitx2c*, paired-like homeodomain 2c; Psmd4b, proteasome 26S subunit, non-ATPase 4b; RING, Really Interesting New Gene; Rpn10, regulatory particle non-ATPase 10; SDF-1, stromal-cell–derived factor 1; Smad, Sma- and Mad-related Protein; Sox, SRY-box transcription factor; spaw, southpaw; T102, threonine 102; *Tg*, transgene; Ub, ubiquitin; UBL, Ub-like; WISH, whole-mount in situ hybridization; Wnt, wingless/integrated; zCdt1, zebrafish chromatin licensing and DNA replication factor 1; zFoxj1a, zebrafish Foxj1a; α-Tubulin, acetylated tubulin.

the ciliated LRO is referred to as Kupffer's vesicle (KV), which forms from dorsal forerunner cells (DFCs), a group of superficial cells in the organizer region of the gastrula [2, 3]. It has been well established that the architecture of KV cells and asymmetric KV cilia generate a counterclockwise nodal flow. This leads to the asymmetrical expression of early laterality genes, including *nodal*-related *southpaw* (*spaw*) and *paired-like homeodomain 2c* (*pitx2c*) in the left lateral plate mesoderm (LPM), and ultimately the establishment of L–R asymmetric patterning [4]. The origin of L–R asymmetry is conserved across many vertebrates, and defects in the establishment of these asymmetries can result in a broad spectrum of birth defects, often including congenital heart malformations [5, 6].

The progression of cells through the G1 and S phases of the cell cycle is tightly controlled by the sequential activation of a family of serine–threonine kinases known as the cyclin-dependent kinases (CDKs). CDK4 and its homolog CDK6 are activated by D-type cyclins in early to mid-G1 phase, whereas CDK2 is activated by E- and A-type cyclins during the late G1 and S phases, respectively [7]. Recent evidence indicates that cell-cycle dynamics have emerged as a key regulator of stem cell fate decisions [8–10]. Specifically, Cyclin D proteins have been shown to activate CDK4/6, which restricts the activity of Sma- and Mad-related Protein (Smad) 2/3 in late G1 phase and results in a switch from endoderm to neuroectoderm potential in human pluripotent stem cells [11]. The G1 cyclin proteins together with their associated CDKs also play essential, direct roles in the maintenance of cell stemness and in the regulation of cell fate specification in mouse embryonic stem (ES) cells by phosphorylation and stabilization of the core pluripotency factors, Nanog homeobox (Nanog), SRY-box transcription factor (Sox) 2, and Octamer-binding protein 4 (Oct4) [12]. In addition, CDK4/Cyclin D1 overexpression has been shown to prevent G1 lengthening and functions to inhibit neurogenesis in mouse embryos [13]. In zebrafish, DFCs vigorously proliferate and collectively migrate towards the vegetal pole during epiboly stages. They then cluster and differentiate into polarized epithelial cells of KV [4, 14, 15]. Interestingly, DFC proliferation defects are often accompanied by impaired cilia elongation in KV [16–18], indicating a possible connection between cell-cycle events and KV cilia formation. However, the underlying mechanism remains poorly understood.

Foxj1, a forkhead-domain–containing transcription factor that is expressed in various ciliated tissues, has been associated with motile cilia formation and L–R axis development in mammals [19, 20]. In zebrafish, two *foxj1* paralogs have been identified, including forkhead box j1a (*foxj1a*) and *foxj1b* [21]. *foxj1a* has been shown to be highly expressed in the DFCs toward the end of gastrulation and plays a primary role in KV ciliogenesis, while *foxj1b* is expressed in the otic vesicle, where it has been shown to regulate motile cilia formation [21, 22]. The expression level of *foxj1a* transcripts has been shown to be regulated by the Hedgehog, wingless/integrated (Wnt)/β-catenin, and fibroblast growth factor (FGF) signaling pathways [17, 21, 23]. Ligand of numb-protein X 2b (Lnx2b)—a Really Interesting New Gene (RING) domain containing E3 ubiquitin (Ub) ligase, which is specifically expressed in the migratory DFCs and developing KV—plays a critical role in the establishment of L–R laterality. This indicates the involvement of protein ubiquitination in the determination of L–R asymmetry [24]. However, whether the function of Foxj1 protein in KV ciliogenesis is regulated by Ub modification remains unknown.

Chemokines are small (8–14 kDa), vertebrate-specific proteins that can be categorized into four subgroups according to the presence and position of conserved cysteine residues (C, CC, CXC, and CX3C) [25]. Among chemokines of the CXC class, the stromal-cell–derived factor 1 (SDF-1/CXCL12) and its receptor CXCR4, which were first identified because of their primary role in leukocyte homing, have been implicated in the regulation of cell adhesion and migration during embryonic development [25–27]. Interestingly, in zebrafish, two Cxcl12 ligands

and two Cxcr4 receptors were found to be expressed across a wide range of cell types and developmental stages and were found to act as discrete pairs to direct cell migration [26]. Cxcl12a–Cxcr4b signaling controls processes such as the directional migration of primordial germ cells, the collective migration of the lateral line primordium, and the formation of the trunk lymphatic network [28–30]. On the other hand, the Cxcl12b–Cxcr4a axis has been shown to play a role in endodermal morphogenesis, vascular system patterning, and the migration and prechondrogenic condensation of cranial neural crest cells [31–34]. It has been shown previously that *cxcr4a* and *cxcr4b* possess mutually exclusive expression patterns in the majority of cell lineages [35]. For example, *cxcr4a*, but not *cxcr4b*, is expressed in the primordium of KV [35]. While *cxcr4b* expression reveals an asymmetric pattern in habenular neurogenesis, the *cxcr4b* mutant *odysseus* displays no obvious phenotype in L–R epithalamic asymmetry [36]. These observations bring into question whether the signaling cascades initiated by Cxcl12b and Cxcr4a play a role in the establishment of L–R asymmetry.

Here, we provide evidence suggesting that the Cxcl12b–Cxcr4a axis is essential for L–R asymmetric development. *Cxcr4a*^{um20} mutants were found to exhibit poor DFC proliferation and abnormal KV cilia formation. Specifically, depletion of *cxcr4a* in DFCs was found to lead to a significant decrease in ERK1/2 signal activation, which was essential for the expression of *cyclin D1*. Subsequent biochemical and functional approaches demonstrated that Cyclin D1–CDK4/6 functions to accelerate the G1/S transition to promote DFC proliferation and stabilize Foxj1a for cilia formation. Mechanistically, CDK4 phosphorylates Foxj1a at T102 and then disrupts its association with Psmd4b, which in turn prevents the Ub-independent proteasomal degradation of Foxj1a protein. Therefore, Cxcl12b–Cxcr4a chemokine signaling links cell-cycle progression and cilia formation for L–R symmetry breaking via regulating Cyclin D1 expression.

Results

Cxcl12b–Cxcr4a axis is required for L–R laterality

cxcr4a was previously found to be expressed in KV progenitors at the end of gastrulation [35]. To address the detailed expression patterns of *cxcr4a*, whole-mount in situ hybridization (WISH) was carried out during early zebrafish embryogenesis. As shown in S1A Fig, *cxcr4a* expression was observed in endoderm cells and migrating DFCs throughout gastrulation. At early somite stages, concomitant with the onset of anterior neural plate expression, *cxcr4a* was also found to be activated in the developing KV cells besides the central lumen (S1B Fig). Therefore, we hypothesized that *cxcr4a* might play a critical role in KV organogenesis and L–R asymmetric patterning.

We then set out to test whether *cxcr4a* is required for L–R development. *cxcr4a*^{um20} mutant carries a null mutation in the *cxcr4a* gene, which causes an in-frame 5-amino–acid deletion within the second transmembrane domain of the Cxcr4a receptor that eliminates its membrane localization [34]. To generate homozygous *cxcr4a* mutants, about 200 of the offspring from heterozygous *cxcr4a*^{um20} parents were bred and maintained to sexual maturity, but only a few of homozygous mutants were identified, suggesting most of them could not survive up to adulthood. As previously reported, the maternal-zygotic *cxcr4a* (MZ*cxcr4a*) mutant embryos generated by incrossing homozygous *cxcr4a*^{um20} adults exhibited distinct defects in lateral dorsal aorta formation (S1C Fig) [34]. Hereinafter, if not specially mentioned, the terms *cxcr4a*^{um20} mutant or *cxcr4a*^{um20} embryo refers to the MZ*cxcr4a* mutant. In order to analyze the laterality information in *cxcr4a*^{um20} mutants, we examined cardiac development by WISH against cardiac myosin light chain 2 (*cmlc2*). At 48 hours postfertilization (hpf), the majority of wild-type embryos showed a heart tube looping to the right (D-loop) (Fig 1A and 1B).

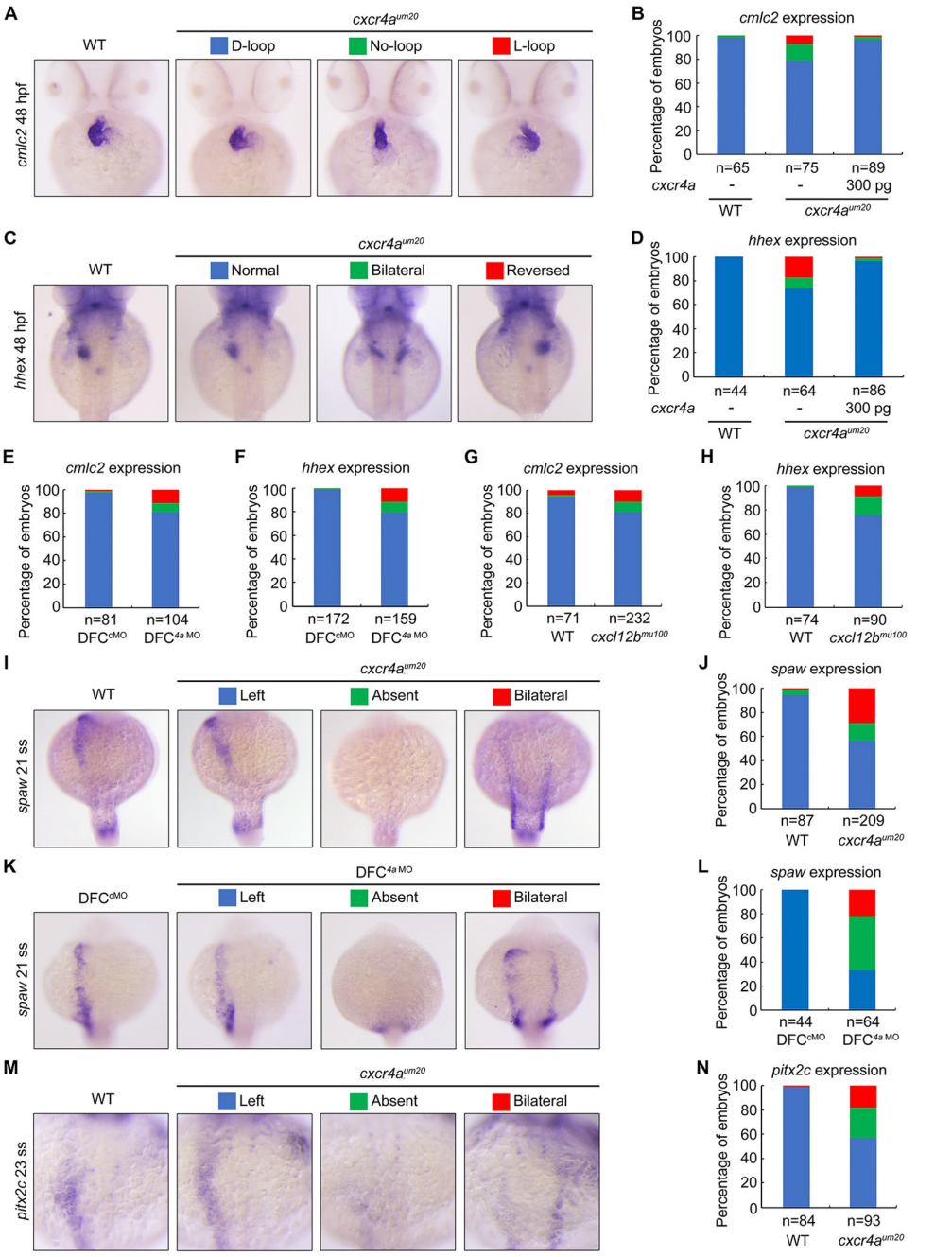

Fig 1. Cxcl12b–Cxcr4a signaling axis is essential for L–R asymmetric development. (A–D) WT embryos and *cxcr4a*^{um20} mutants injected with or without 300 pg *cxcr4a* mRNA at the 256-cell stage were examined for cardiac looping and liver laterality at 48 hpf by WISH against *cmlc2* (A) and *hhex* (C). Embryos with different phenotypes are shown in ventral (A) or dorsal view (C), and the ratios are shown in (B) and (D). Underlying data can be found in S1 Data. (E–H) Embryo ratios with different expression patterns of *cmlc2* and *hhex* at 48 hpf in WT embryos injected with 8 ng *cxcr4a* MO (*4a* MO) at the 256-cell stage (E and F) and *cxcl12b* mutants (G and H). Underlying data can be found in S1 Data. (I–N) *cxcr4a* deficiency alters Nodal gene expression pattern. Representative images of *spaw* and *pitx2c* expression in *cxcr4a* mutants (I and M) and morphants (K). All embryos are shown in dorsal views with anterior on the top. Ratios of embryos are shown in (J), (L), and (N). Underlying data can be found in S1 Data. *cmlc2*, cardiac myosin light chain 2; DFC, dorsal forerunner cell; *hhex*, hematopoietically expressed homeobox; hpf, hours postfertilization; L–R, left–right; MO, morpholino; *pitx2c*, *paired-like homeodomain 2c*; *spaw*, *southpaw*; WISH, whole-mount in situ hybridization; WT, wild-type.

https://doi.org/10.1371/journal.pbio.3000203.g001

However, the heart localization was mildly affected in *cxcr4a*^{um20} mutants, of which 21% showed a "no-looping" or reversed "left-looping" heart (L-loop) (Fig 1A and 1B). Moreover, about 30% of *cxcr4a*^{um20} embryos also exhibited disrupted liver position, as revealed by *hematopoietically expressed homeobox* (*hhex*) expression (Fig 1C and 1D). In addition, these L–R laterality defects were well rescued by injection of 300 pg *cxcr4a* mRNA into embryonic yolk at the midblastula stage (256-cell stage) (Fig 1B and 1D; S3A and S3B Fig), which would lead to a specific overexpression of *cxcr4a* in DFC/KV cells [37]. Conversely, we did not observe any rescue effect with the overexpression of *cxcr4a*^{um20}, which contains the 5-amino–acid in-frame deletion (S2A and S2B Fig). Thus, *cxcr4a* is important for organ laterality in zebrafish embryos. Interestingly, when MZ*cxcr4a* mutant adult females were mated to wild-type male fish, the resultant embryos (maternal *cxcr4a* mutants) displayed normal asymmetry of the heart and liver (S3A and S3B Fig). In contrast, zygotic *cxcr4a*^{um20} homozygous mutants, which were identified from *cxcr4a*^{um20} heterozygous fish crosses by genotyping, had similar L–R defects as MZ*cxcr4a* embryos (S3C and S3D Fig). Therefore, these data suggest that the zygotic, but not maternal, *cxcr4a* function is required for L–R asymmetric development.

Because *cxcr4a* depletion would impair endoderm cell migration during gastrulation and cause bilateral duplication of endodermal organs such as the liver [31], we injected a previously validated morpholino (MO) that targets *cxcr4a* (*4a* MO) at the midblastula stage to specifically block *cxcr4a* activity in DFC/KV cells. In comparison to injection with a standard control MO (cMO), injection of *4a* MO led to similar laterality abnormalities as observed in *cxcr4a*^{um20} mutants (Fig 1E and 1F). This suggests that the organ localization defects are not secondary effects of impaired endoderm migration. Therefore, the *cxcr4a* expression in DFC/KV cells is required for L–R laterality. In addition, the deficiency of *cxcl12b* in *cxcl12b*^{mu100} mutants [38] was also found to result in laterality defects (Fig 1G and 1H), indicating that the Cxcl12b–Cxcr4a signaling pathway is critical for L–R symmetry breaking.

Because organ laterality is regulated by evolutionally conserved asymmetric L–R gene expression in vertebrates, we next examined the expression patterns of *spaw* and its downstream gene *pitx2c* [1, 39]. At the late somite stages, we observed *spaw* and *pitx2c* expression in the left LPM in wild-type embryos, whereas expression of these genes was found to be bilateral or absent in *cxcr4a*^{um20} mutants and DFC$^{4a\ MO}$ embryos (Fig 1I–1N). Interestingly, the bilateral expression domain of *spaw* in a subset of *cxcr4a*^{um20} mutants was located in the more posterior region in the LPM (Fig 1I), indicating a delay in the anterior spreading of *spaw* expression.

Collectively, these results demonstrate a sustaining expression of *cxcr4a* in the DFC/KV cells and implicate a crucial role of Cxcl12b–Cxcr4a chemokine signaling in L–R laterality determination.

Ablation of *cxcr4a* compromises KV organogenesis and ciliogenesis

To determine whether a loss of *cxcr4a* alters KV morphogenesis, we first examined the formation of DFC clusters during gastrulation in *cxcr4a*^{um20} mutants carrying the transgenic DFC/KV reporter *sox17:green fluorescent protein* (*GFP*). We observed that in both wild-type embryos and *cxcr4a*^{um20} mutants, the GFP-positive DFCs were maintained as a cohesive group and migrated towards the vegetal pole during mid to late gastrulation (S4A Fig). Meanwhile, in comparison to control embryos, *cxcr4a*^{um20} mutants exhibited a normal expression pattern of *sox17* transcripts in the DFC clusters (S4B Fig). Based on these observations, we concluded that *cxcr4a* is unnecessary for the specification, clustering, and collective migration of DFCs.

We then examined the morphology of KV in live embryos at the 10-somite stage, at which point KV was well formed [4]. Wild-type embryos exhibited a normal button-like KV at the

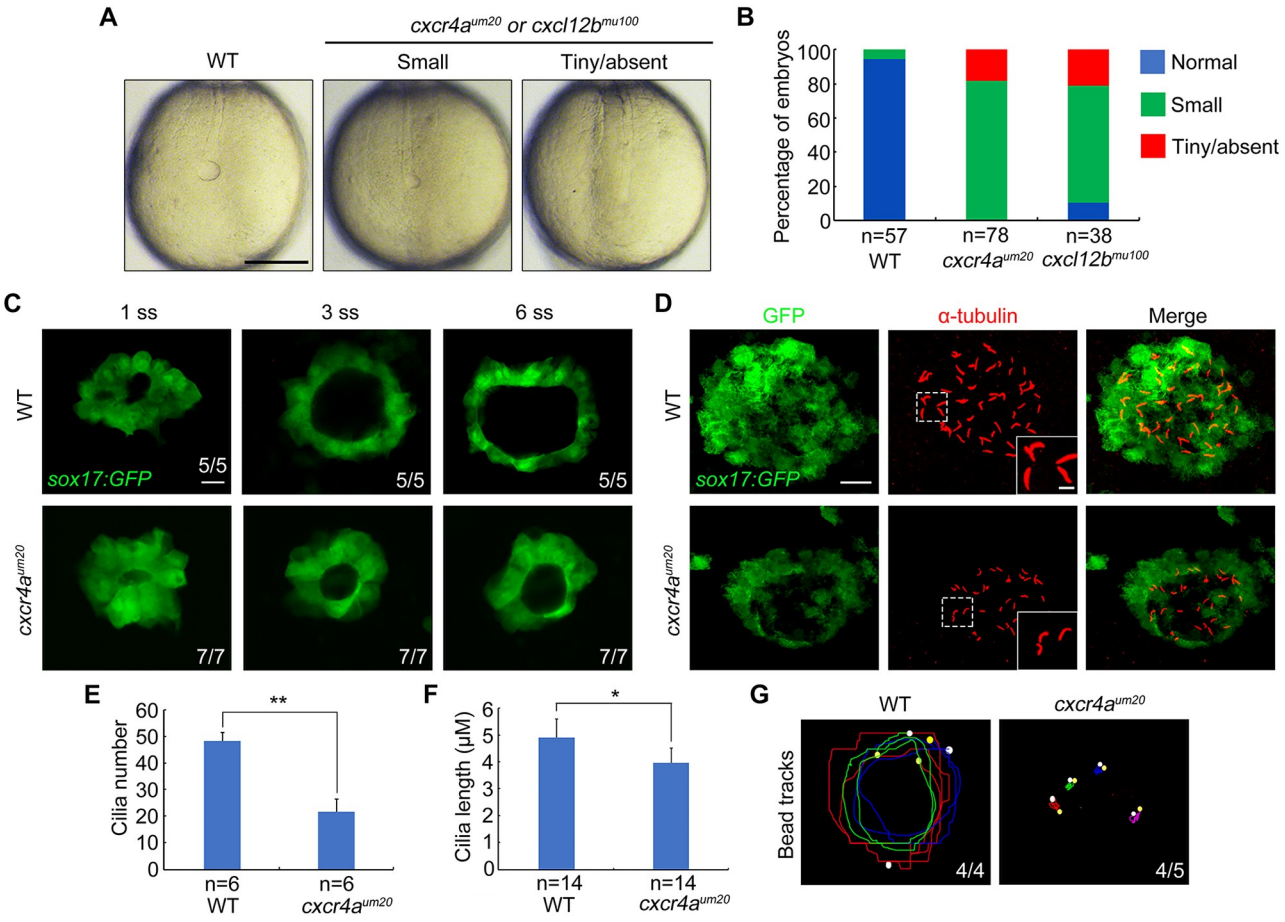

Fig 2. *cxcr4a* is indispensable for KV formation and ciliogenesis. (A–B) Light micrographs at the 10-somite stage showed smaller or even absent KVs in *cxcr4a*^{um20} or *cxcl12b*^{mu100} mutants. Scale bar, 200 μm. Embryo ratios with different KV sizes were shown in (B). Underlying data can be found in S1 Data. (C) Time-lapse confocal images from the 1-somite stage to the 6-somite stage showed the dynamic formation of KV in WT and *cxcr4a*-deficient *Tg(sox17:GFP)* embryos. Scale bar, 20 μm. The ratios of affected embryos were indicated. (D–F) Fluorescent immunostaining of KV using anti-GFP and anti-α-Tubulin antibodies at the 10-somite stage in WT embryos and *cxcr4a*^{um20} mutants. The boxed areas in the images were presented at higher magnification in the relevant insets. Scale bar, 20 μm. Cilia average number and length were quantified from three independent experiments, and the group values were expressed as the mean ± SD (E and F). Student *t* test, $^{*}P < 0.05$, $^{**}P < 0.01$. Underlying data can be found in S1 Data. (G) Fluorescent bead tracking experiments showed that fluorescent beads moved in a persistent counterclockwise fashion in WT embryos but had no directional flow in *cxcr4a*^{um20} mutants. White spots, yellow spots, and curves mark the start points, the end points, and the tracks of bead movements, respectively. GFP, green fluorescent protein; KV, Kupffer's vesicle; *sox*, SRY-box transcription factor; *Tg*, transgene; WT, wild-type; α-Tubulin, acetylated tubulin.

https://doi.org/10.1371/journal.pbio.3000203.g002

terminus of the notochord, as observed under bright-field microscopy (Fig 2A). In contrast, a large majority of *cxcr4a*^{um20} mutants displayed a smaller or tiny/absent KV (Fig 2A and 2B). Consistently, similar defects in KV morphology were found in *cxcl12b*^{mu100} mutants (Fig 2A and 2B). In order to monitor the dynamic changes during KV formation, we carried out in vivo time-lapse image analysis on *cxcr4a*-deficient transgene (Tg) *sox17:GFP* embryos from the 1- to 6-somite stages. DFCs were found to have already rearranged into a single rosette concurrent with the formation of the preliminary lumen in 1-somite–stage wild-type and *cxcr4a*^{um20} mutant embryos (Fig 2C). However, the GFP-positive KV appeared to be dramatically smaller in *cxcr4a*^{um20} embryos in comparison to control animals from the 3- to 6-somite stages (Fig 2C). We next looked into the apical–basal polarity of KV epithelial cells, which is critical for the correct establishment of L–R asymmetry [40]. Immunostaining experiments revealed that the distributions of the basal–lateral marker E-cadherin and the apical marker

atypical protein kinase C (aPKC) in KV epithelial cells of 10-somite–stage *cxcr4a*^{um20} embryos were correct (S4C and S4D Fig). These observations suggest that *cxcr4a* is critical for organ size control but is not required for epithelial cell polarization during KV organogenesis.

Monocilia in KV are known to generate a counterclockwise fluid flow, which creates the asymmetrical signals required to break L–R symmetry [4]. We next analyzed KV cilia formation by probing acetylated tubulin (α-Tubulin) in the *cxcr4a*^{um20} embryos at the 10-somite stage. We found that in comparison with control embryos, *cxcr4a*^{um20} mutants exhibited a significant decrease in cilia number and a steady reduction in cilia length (Fig 2D–2F). As expected, *cxcl12b*^{mu100} mutant embryos showed similar abnormalities in ciliogenesis (S5A–S5C Fig). We then sought to determine whether the KV directional fluid flow was altered in *cxcr4a*^{um20} mutants. Fluorescent beads were injected into KVs at the 6-somite stage, and the movements of the beads were tracked at the 10-somite stage. The fluorescent beads moved in a persistent counterclockwise fashion in wild-type embryos, whereas they exhibited no directional flow in *cxcr4a*-deficient embryos (Fig 2G; S1 and S2 Movies). Interestingly, *cxcr4a*^{um20} mutants exhibited no obvious defects in the KV cilia motility as revealed by high-speed video microscopy (S3 and S4 Movies), indicating that the impaired fluid flow in KVs is primarily resulted from the reduction in the number and length of motile cilia. Therefore, these results indicated that *cxcr4a* is indispensable for KV ciliogenesis and cilia-driven fluid flow.

Absence of *cxcr4a* attenuates G1/S transition and zFoxj1a protein expression

Our studies suggest that *cxcr4a* deficiency leads to smaller KV size as well as fewer KV cilia. Interestingly, the majority of the KV epithelial cells in *cxcr4a* mutants exhibited an intact apical–basal polarity and formed notably shortened cilia (Fig 2D; S4C and S4D Fig). This suggests that the altered KV cilia numbers may be caused by defects in cell proliferation. To address this issue, we first examined the proliferation profile of DFC/KV cells by performing bromodeoxyuridine (BrdU) incorporation assays in *Tg(sox17:GFP)* embryos during gastrulation and early somite stages. Consistent with previous reports [16], approximately 70% of DFCs were positively stained with BrdU at the midgastrulation stage, whereas very few BrdU-positive cells were observed in the developing KV at the bud and the 6-somite stages (Fig 3A and 3B), suggesting that vigorous proliferation occurs in DFCs during epiboly stages and then declines at the end of gastrulation. Impressively, we found a dramatic decrease of the BrdU-positive DFC number in *cxcr4a*-deficient embryos at midgastrulation stage (Fig 3C and 3D), indicating a crucial requirement of *cxcr4a* in DFC proliferation.

We next examined the detailed effects of *cxcr4a* deficiency on DFC cycle progression in *Tg(sox17:GFP;EF1α:mKO2-zCdt1(1/190))* double transgenic embryos, a model in which cells in G1 phase exhibit red nuclear fluorescence [41]. Because the G1/S transition is very short in cells that undergo rapid mitotic cycles [41], we were unable to identify any mKO2-zCdt1–positive DFCs in both control embryos and *cxcr4a*^{um20} mutants during gastrulation. Interestingly, while the majority of cells in the developing KV enter into a quiescent state at the end of gastrulation (Fig 3A and 3B), we observed no or only few KV progenitors with mKO2-zCdt1 fluorescence in wild-type embryos at the bud and 3-somite stages (Fig 3E–3H). These results, combined with the previous observation that the mKO2-zCdt1 signal was highlighted in differentiated cells—including postmitotic neurons and muscle cells from the 10-somite stage [41]—imply that there exist limitations in the ability to dissect cell-cycle behavior using this fluorescent indicator in early zebrafish embryos. However, *cxcr4a*^{um20} mutant embryos showed a marked proportion of KV progenitors with robust mKO2-zCdt1 expression, indicating impaired G1/S transition and an apparent lengthening of the G1 phase (Fig 3E–3H).

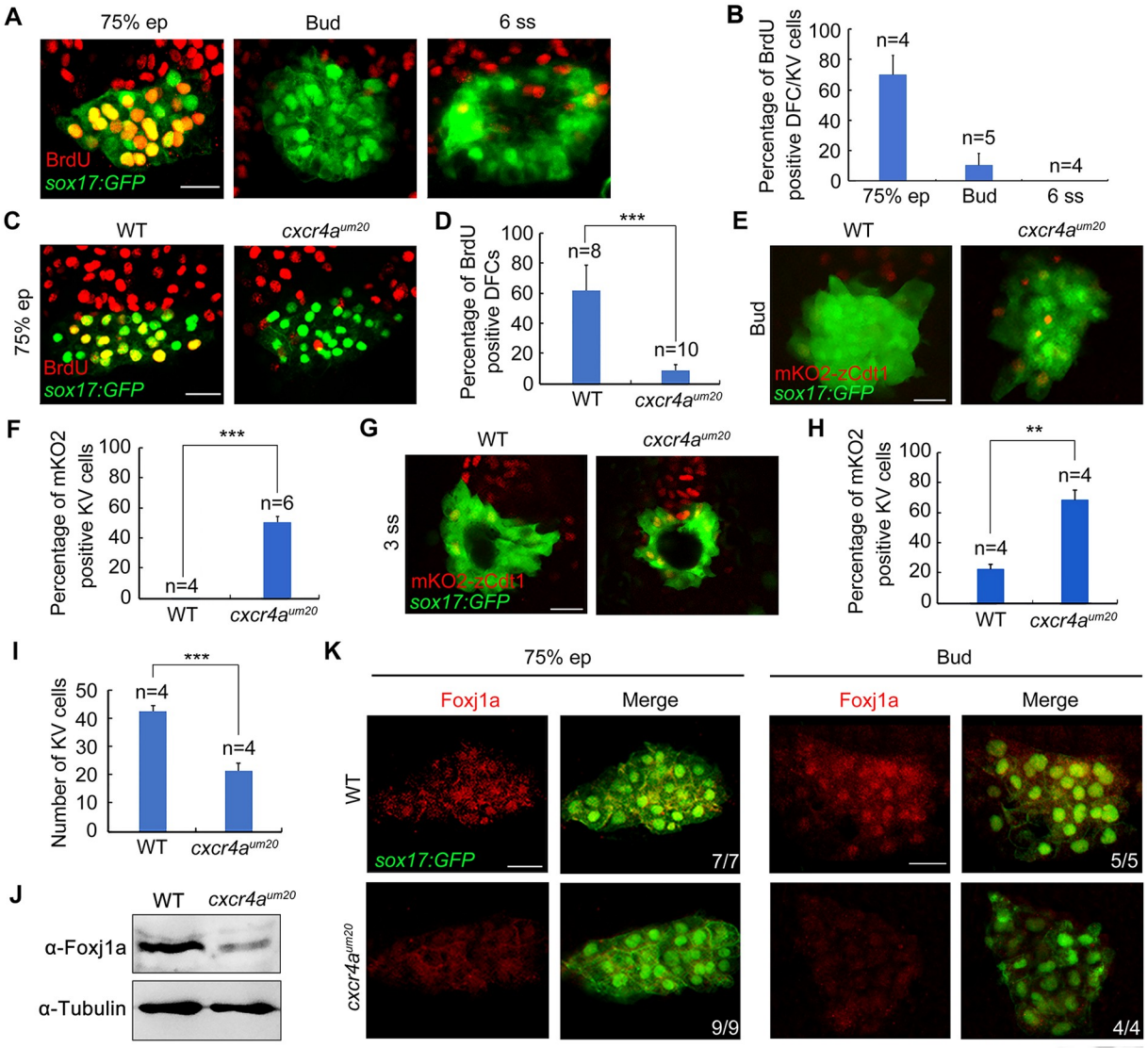

Fig 3. Depletion of *cxcr4a* impairs G1/S transition and Foxj1a protein expression in DFCs. (A–B) Representative confocal sections of BrdU-positive DFCs and KV cells at the indicated stages (A). Dorsal views with anterior on the top. Scale bar, 20 μm. The percentage of BrdU-positive cells among GFP-positive DFCs and KV cells were quantified from the indicated embryo numbers in three independent experiments, and the group values are expressed as the mean ± SD (B). Underlying data can be found in S1 Data. (C-D) BrdU incorporation experiments showed reduced proliferating DFCs in *cxcr4a*^{um20} mutants at the 75% epiboly stage. Scale bar, 20 μm. Statistical data from three independent experiments are shown in (D). Student *t* test, $^{***}P < 0.001$. Underlying data can be found in S1 Data. (E–I) Depletion of *cxcr4a* inhibits the G1/S transition in DFCs. Representative confocal sections of WT and *cxcr4a*-deficient *Tg(sox17:GFP;EF1α:mKO2-zCdt1(1/190))* embryos at the bud and 3-somite stages are shown in (E) and (G). Dorsal views with anterior to the top. Scale bar, 20 μm. The percentage of mKO2-positive KV cells were quantified from three independent experiments (F and H). The average numbers of KV cells in WT embryos and *cxcr4a*^{um20} mutants at the 3-somite stage are shown in (I). The significance of differences compared with the WT group was analyzed with the Student *t* test, $^{**}p < 0.01$; $^{***}p < 0.001$. Underlying data can be found in S1 Data. (J–K) *cxcr4a* deficiency down-regulates zFoxj1a protein expression levels. WT and *cxcr4a*-deficient *Tg(sox17:GFP)* embryos were harvested at the 75% epiboly and bud stages and then subjected to western blot analysis (J) and immunostaining (K) with the indicated antibodies. Scale bar, 20 μm. BrdU, bromodeoxyuridine; DFC, dorsal forerunner cell; Ef1α, eukaryotic translation elongation factor 1α; ep, epiboly; Foxj1a, forkhead box j1a; GFP, green fluorescent protein; KV, Kupffer's vesicle; mKO2, monomeric Kusabira Orange2; *sox*, SRY-box transcription factor; *Tg*, transgene; WT, wild-type; zCdt1, zebrafish chromatin licensing and DNA replication factor 1; zFoxj1a, zebrafish Foxj1a; α-Tubulin, acetylated tubulin.

https://doi.org/10.1371/journal.pbio.3000203.g003

When *cxcr4a* in DFCs was knocked down, similar defects in cell-cycle progression were found (S6A–S6D Fig). Besides, consistent with the smaller KVs in *cxcr4a*-deficient embryos during early somite stages (Fig 2C), we found that the number of KV cells declined about 50% in *cxcr4a*^{um20} mutants at the 3-somite stage compared with that of wild-type controls (Fig 3G and 3I). Nevertheless, our results suggest that Cxcr4a-mediated chemokine signaling is responsible for driving DFC proliferation by accelerating the G1/S transition. This provides an explanation for the smaller KV size that was observed in *cxcr4a*^{um20} mutants.

Because zebrafish Foxj1a (zFoxj1a) is a master regulator of KV ciliogenesis [21, 22], we then sought to determine whether zFoxj1a expression was affected in *cxcr4a*^{um20} mutants. In situ hybridization analysis demonstrated normal expression levels of *foxj1a* transcripts in *cxcr4a*^{um20} embryos during gastrulation (S7 Fig). To examine the changes of zFoxj1a protein expression in *cxcr4a*^{um20} embryos, we first validated the reliability of an antibody against human FOXJ1 in *foxj1a* morphants. Western blotting revealed a specific protein band corresponding to zFoxj1a protein (about 70 kDa) in the lysates from 75%-epiboly–stage embryos injected with cMO, which was drastically reduced in the lysates from *foxj1a* morphants (S8A Fig). Moreover, results of immunofluorescent assays showed a clear expression of zFoxj1a protein in the floor plate of the spinal cord, as well as the pronephric ducts of control embryos, at 24 hpf (S8B and S8C Fig). In contrast, zFoxj1a protein expression was markedly attenuated in these tissues upon *foxj1a* MO injection (S8B and S8C Fig), indicating that the antibody we used can specifically recognize endogenous zFoxj1a protein. Subsequently, we found a clear decrease of zFoxj1a protein expression in *cxcr4a*^{um20} mutants as revealed by western blot and immunostaining experiments (Fig 3J and 3K). These analyses provide strong evidence that Cxcr4a signaling is responsible for controlling KV ciliogenesis through regulation of zFoxj1a protein expression at the post-transcription level.

Cxcr4a–ERK1/2 cascade controls DFC proliferation by regulating Cyclin D1 expression

The Cxcl12–Cxcr4 axis is known to regulate cell-cycle progression through glycogen synthase kinase 3β (GSK-3β)/β-catenin and ERK1/2 signaling pathways [42–44]. To determine which of these candidate pathways mediates Cxcr4-regulated DFC proliferation, *cxcr4a*^{um20} mutant embryos were immunostained with antibodies against β-catenin or phosphorylated ERK1/2 (p-ERK1/2) at the 75% epiboly stage. No obvious changes in the cellular distribution of endogenous β-catenin in DFCs were observed in *cxcr4a*^{um20} mutants (S9 Fig), indicating that GSK-3β/β-catenin signaling is not altered with *cxcr4a* depletion. However, we found a robust expression of p-ERK1/2 in wild-type DFCs that was nearly abolished in *cxcr4a*-deficient cells (Fig 4A). Strikingly, DFC-specific overexpression of *MEK1*$^{S219D,\ S223D}$, a constitutively activated version of MEK1 (caMEK1) [45], rescued the L–R defects in *cxcr4a*^{um20} mutants in a dose-dependent manner (Fig 4B–4E). Therefore, these results demonstrate a role for ERK1/2 signaling downstream of Cxcr4 in organ laterality.

Among the cell-cycle–regulatory genes, Cyclin D1 expression is known to be specifically activated by the Cxcr4a–ERK1/2 cascade to promote cell proliferation [42, 43, 46]. Consistent with these previous studies, double fluorescence in situ hybridization analyses indicated a dramatic reduction in *cyclin D1* expression in *cxcr4a*-deficient DFCs (Fig 4F). In addition, the introduction of caMEK mRNA counteracted the *cxcr4a* depletion effects on *cyclin D1* expression (Fig 4F). Cell-cycle progression from G1 to the S phase is governed by CDK4/6 and CDK2, which are activated by D-type and E- or A-type cyclins, respectively [7]. To investigate the connections between cell-cycle progression and organ laterality, *Tg(mKO2-zCdt1(1/190))* embryos were treated with a selective CDK4/6 inhibitor PD0332991 and a specific CDK2

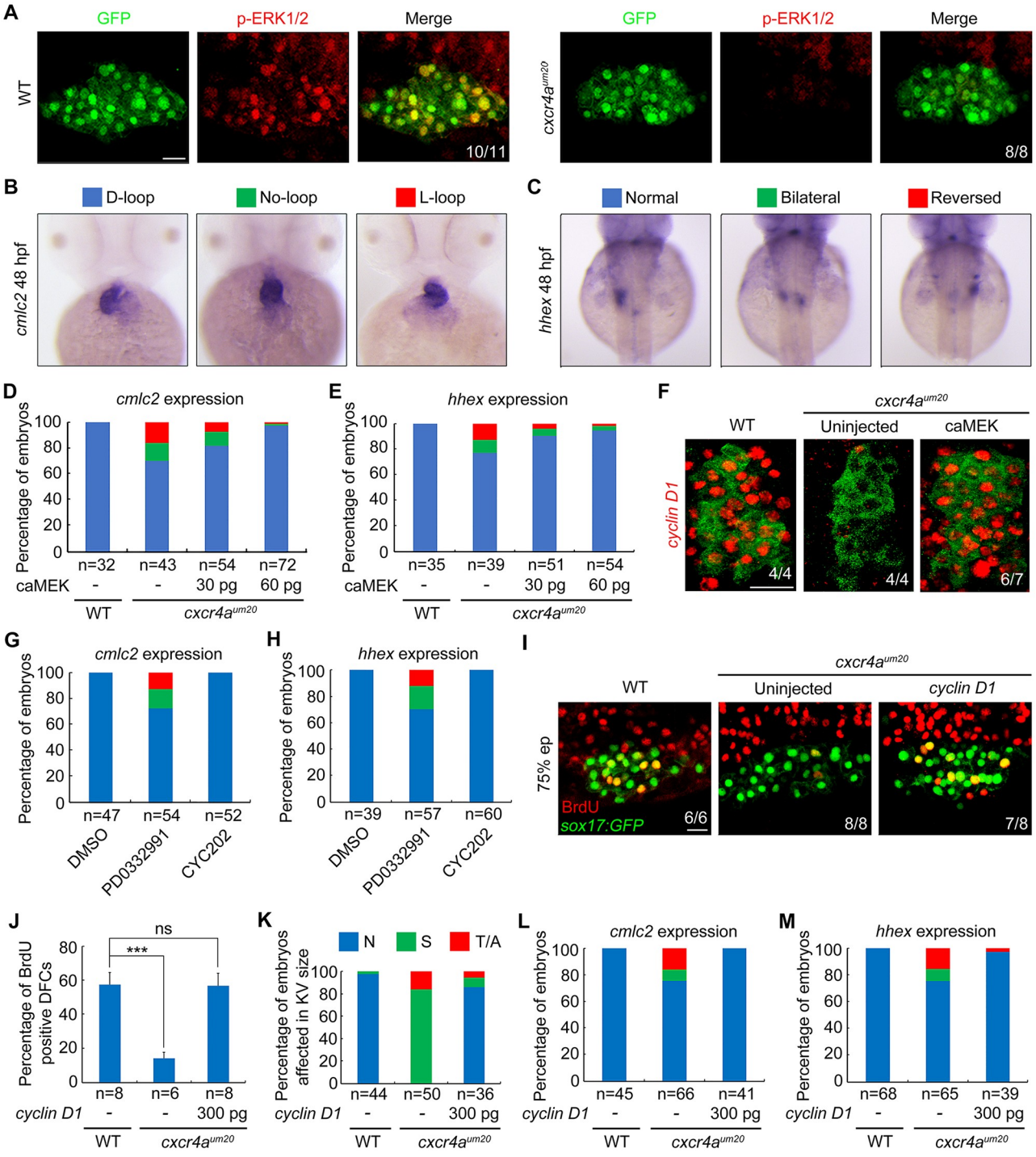

Fig 4. Cxcr4 promotes Cyclin D1 expression through ERK signaling during DFC proliferation. (A) ERK1/2 phosphorylation levels were dramatically decreased in *cxcr4a*^{um20} mutants. WT and *cxcr4a*-deficient *Tg(sox17:GFP)* embryos were harvested at the 75% epiboly stage and subjected to immunostaining for p-ERK1/2 (red) and GFP (green). All embryos are shown in dorsal views with anterior to the top. Scale bar, 20 μm. (B–E) caMEK mRNA overexpression in DFCs rescued L–R patterning defects in *cxcr4a*^{um20} mutants. Different types of heart looping and liver laterality at 48 hpf in *cxcr4a*^{um20} mutants following midblastula injection of different caMEK mRNA doses were visualized by *cmlc2* and *hhex* expression (B and C). The ratios are shown in (D) and (E). Underlying data can be found in S1 Data. (F) *Cxcr4a*-deficient *Tg(sox17:GFP)* embryos were injected with 60 pg caMEK mRNA at the 256-cell stage and then harvested at the 75% epiboly stage for fluorescence in situ hybridization experiments with *cyclin D1* (red) and GFP (green) probes. Dorsal views with anterior to the left. Scale bar, 20 μm. (G–H) WT embryos were treated with 0.5 μM PD0332991 or 0.2 μM CY202 from the shield stage to bud stage and then analyzed for L–R patterning defects at 48 hpf by in situ hybridizations with *cmlc2* and *hhex* probes. The proportion of treated embryos exhibiting each type of heart looping and liver laterality is shown in (G) and (H). Underlying data can be found in

S1 Data. (I–J) Reintroduction of *cyclin D1* into DFCs relieves DFC proliferation defects in *cxcr4a*^{um20} mutants. *Cxcr4a*-deficient *Tg(sox17:GFP)* embryos were injected with or without 300 pg *cyclin D1* mRNA at the 256-cell stage, followed by coimmunostaining with anti-BrdU (red) and anti-GFP (green) antibodies at the 75% epiboly stage. Representative images are shown in (I), and the percentage of BrdU-positive DFCs is indicated in (J). Scale bar, 20 μm. Student *t* test, $^{***}P < 0.001$. Underlying data can be found in S1 Data. (K–M) The reduced ratios of embryos affected in KV size (K) and *cmlc2* (L) or *hhex* (M) expression show that DFC-specific overexpression of *cyclin D1* rescued the defects of KV formation (K) and L–R patterning (L and M) in *cxcr4a* mutants. Underlying data can be found in S1 Data. BrdU, bromodeoxyuridine; caMEK, constitutively activated version of MEK; *cmlc2*, cardiac myosin light chain 2; DFC, dorsal forerunner cell; ERK, extracellular regulated MAP kinase; GFP, green fluorescent protein; *hhex*, hematopoietically expressed homeobox; hpf, hours postfertilization; KV, Kupffer's vesicle; L–R, left–right; ns, no significant difference; p-ERK1/2, phosphorylated ERK1/2; sox, SRY-box transcription factor; *Tg*, transgene; WT, wild-type.

https://doi.org/10.1371/journal.pbio.3000203.g004

inhibitor CYC202 from the shield stage [47, 48]. Both PD0332991 and CYC202 treatments induced a remarkable increase of the number of cells stagnated at G1 stage in the resulting embryos, indicating the high efficiency of these chemicals in the zebrafish embryos (S10 Fig). Interestingly, upon exposure of wild-type embryos to PD0332991 from the shield stage to the bud stage, the resulting animals exhibited L–R defects similar to those observed in *cxcr4a*^{um20} mutants (Fig 4G and 4H). At the same time, embryos treated with CYC202 showed no significant changes in laterality development (Fig 4G and 4H). These results suggest that Cyclin D1–CDK4/6 complexes play critical roles in DFC proliferation and L–R asymmetric development. Importantly, reintroduction of *cyclin D1* into DFCs was found to relieve the inhibition of cell proliferation, the reduction of KV size, and the defects of organ laterality in *cxcr4a*^{um20} mutants (Fig 4I–4M). Collectively, our data indicate that the Cxcr4a–ERK1/2 cascade functions in DFC proliferation through regulation of Cyclin D1 expression during zebrafish L–R development.

CDK4 and its kinase activity is required for Foxj1 protein stabilization

Because the injection of *cyclin D1* mRNA into DFCs was found to rescue the L–R defects in *cxcr4a*^{um20} mutants (Fig 4L and 4M), we hypothesized that Cyclin D1 acts downstream of Cxcr4a signaling to control both cell proliferation and cilia formation. In support of this hypothesis, upon injection of 300 pg *cyclin D1* mRNA into midblastula-stage *cxcr4a*^{um20} embryos, we observed that both the number and the length of KV cilia were restored (Fig 5A–5C), indicating a role of Cyclin D1 in ciliogenesis. It is surprising that the DFC-specific delivery of *cyclin D1* mRNA was also able to restore the expression of endogenous zFoxj1a protein in *cxcr4a*^{um20} embryos (Fig 5D).

We next aimed to understand whether Foxj1 protein stability is regulated by Cyclin D1–CDK4/6 complexes. As depicted in Fig 5E, *Cyclin D1* or *CDK4* overexpression in HEK293T cells notably increased zFoxj1a expression. This increase in exogenously expressed zFoxj1a was even more apparent when Cyclin D1–CDK4 complexes were ectopically expressed (Fig 5E). We noted that Cyclin D1–CDK4 complexes also showed similar effects on the expression levels of mouse Foxj1 (mFoxj1) (Fig 5F). In combination with our observation of unchanged *foxj1a* transcript expression in *cxcr4a*^{um20} mutants, these results suggest that Cyclin D1–CDK4 complexes may play crucial roles in the prevention of Foxj1a protein degradation. Indeed, we observed that the treatment of MG132, a proteasome inhibitor, but not NH_4Cl, a lysosome inhibitor, or 3-methyladenine (3-MA), a well-characterized inhibitor of autophagy, dramatically stabilized zFoxj1a protein (Fig 5G). In contrast, blocking endogenous CDK activity with PD0332991 treatment was found to result in a clear reduction of zFoxj1a expression (Fig 5H). In addition, the PD0332991-treatment–induced zFoxj1a turnover was completely suppressed by cotreatment with MG132 (Fig 5H). Therefore, Cyclin D1–CDK4 complexes contribute to Foxj1 protein stabilization. To further determine whether CDK4 kinase activity is important for Foxj1 protein stability, we generated a

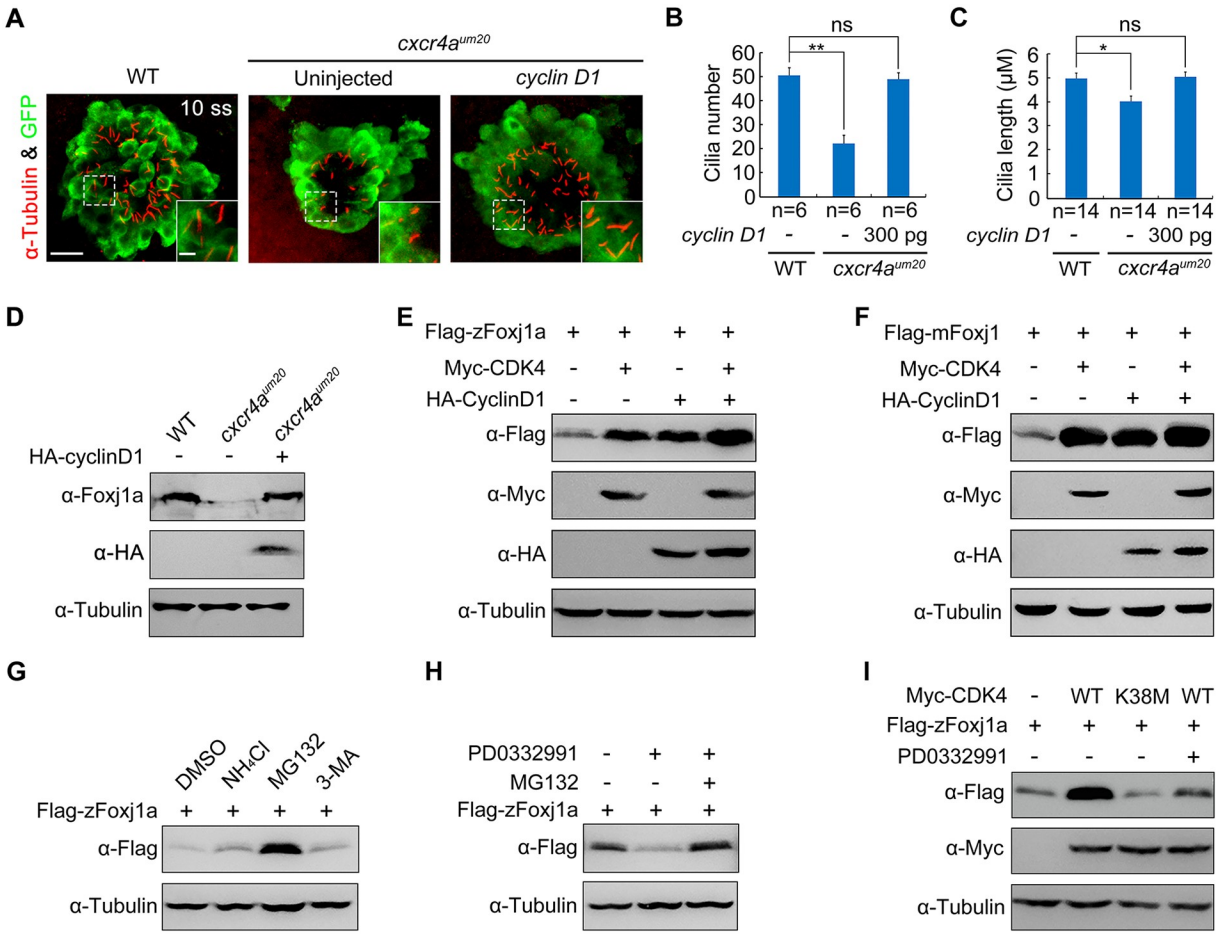

Fig 5. CDK4 stabilizes Foxj1 through its kinase activity. (A–C) Confocal images of 10-somite–stage *cxcr4a*-deficient *Tg(sox17:GFP)* embryos injected with or without 300 pg *cyclin D1* mRNA at the 256-cell stage (A). KV cells were labeled with antibodies against GFP (green), and cilia were visualized by α-Tubulin immunofluorescence (red). The boxed areas in the images are presented at higher magnification in the relevant insets. Scale bar, 20 μm. Cilia number (B) and length (C) were analyzed. Student *t* test, $^{*}P < 0.05$, $^{**}P < 0.01$. Note that when *cyclin D1* mRNA was injected into *cxcr4a*-deficient DFCs, both the KV cilia number and length were restored. Underlying data can be found in S1 Data. (D) Western blots of total lysates from 75%-epiboly–stage WT embryos and *cxcr4a*^{um20} mutants injected with or without 300 pg *HA-cyclin D1* mRNA at the 256-cell stage. Tubulin was used as the loading control. Endogenous zFoxj1a protein levels in *cxcr4a*^{um20} mutants was rescued by DFC-specific overexpression of *HA-cyclin D1*. (E–F) *CDK4* overexpression alone or together with *Cyclin D1* results in an obvious increase in zFoxj1a (E) or mFoxj1 (F) expression. HEK293T cells were transfected with the indicated plasmids. Lysates were analyzed by western blot using the indicated antibodies. (G) HEK293T cells transfected with plasmids encoding Flag-zFoxj1a were treated with the lysozyme inhibitor NH4Cl (20 mM) or the proteasomal inhibitor MG132 (20 μM) or the autophagy inhibitor 3-MA (5 mM) for 5 hours prior to harvest for immunoblotting. (H) Lysates from Flag-zFoxj1a–expressing HEK293T cells treated with CDK4/6 inhibitor PD0332991 (0.5 μM) alone or in combination with MG132 (20 μM) were subjected to immunoblotting. (I) Overexpression of WT *CDK4*, but not its kinase-deficient mutant, stabilizes zFoxj1a protein. HEK293T cells were transfected with the indicated plasmids. PD0332991 (0.5 μM) was added 5 hours before harvest. Note that PD0332991 treatment blocked CDK4-induced zFoxj1a stabilization. CDK, cyclin-dependent kinase; DFC, dorsal forerunner cell; Foxj1a, forkhead box j1a; GFP, green fluorescent protein; HA, hemagglutinin; HEK, human embryonic kidney; KV, Kupffer's vesicle; mFoxj1, mouse Foxj1; mouse Foxj1; sox, SRY-box transcription factor; Tg, transgene; WT, wild-type; zFoxj1a, zebrafish Foxj1a; 3-MA, 3-methyladenine; α-Tubulin, acetylated tubulin.

https://doi.org/10.1371/journal.pbio.3000203.g005

zebrafish kinase-deficient mutant denoted CDK4-K38M, in which the ATP-binding site (Lys-38) in the catalytic subunit was mutated to a methionine residue [49]. As shown in Fig 5I, ectopic expression of CDK4-K38M had no effect on the zFoxj1a expression, and PD0332991 treatment eliminated CDK4-mediated protein stabilization. These data suggest that CDK4 stabilizes Foxj1 through its kinase activity.

CDK4 physically interacts with and directly phosphorylates Foxj1

To understand whether Foxj1 is a substrate of CDK4 kinase, we first examined the possible interaction between these two proteins. HeLa cells were transiently transfected with Flag-tagged zFoxj1a and Myc-tagged CDK4. Immunofluorescence staining experiments revealed a colocalization of overexpressed zFoxj1a and CDK4 in the nuclear aggregates (Fig 6A), suggesting a potential interaction between these two proteins. Because zFoxj1a was observed to be localized exclusively to the nucleus even when coexpressed with CDK4 (Fig 6A), we excluded the effects of CDK4 on the subcellular distribution of zFoxj1a. We next examined the association between zFoxj1 and CDK4 in wild-type embryos and HEK293T cells. Coimmunoprecipitation experiments demonstrated that overexpressed CDK4 interacted with endogenous and ectopically expressed zFoxj1a (Fig 6B and 6C). Interestingly, the kinase-deficient form of CDK4 failed to associate with zFoxj1a (Fig 6C). In order to test whether CDK4 interacts directly with Foxj1 protein, we carried out an in vitro binding assay using purified proteins. As depicted in Fig 6D, Myc-CDK4 protein purified from bacterial cells was able to bind to glutathione S-transferase (GST)-zFoxj1a but not GST proteins. Collectively, these results demonstrate that CDK4 interacts directly with zFoxj1a protein.

It is well established that the CDK families of serine/threonine protein kinases phosphorylate substrates containing the consensus amino-acid sequence (S/T)PXR/K [50]. Because Cyclin D1–CDK4 complexes contribute to the stabilization of both mouse and zebrafish Foxj1 (Fig 5E and 5F), we hypothesized that CDK4 is involved in the phosphorylation of Foxj1 within conserved classic substrate motifs. Interestingly, we found that zFoxj1a contains a potential CDK phosphorylation motif "TPGK" at the N-terminal region, which is highly conserved in vertebrates (Fig 6E). To investigate whether CDK4 phosphorylates Foxj1 protein, a phospho-threonine–proline antibody was used to enrich CDK substrates from whole-cell lysates, and the presence of phosphorylated Foxj1 was examined by western blot. With these experiments, we found that CDK4 or Cyclin D1–CDK4 complexes could effectively phosphorylate zFoxj1a and mFoxj1 (Fig 6F; S11A Fig). As expected, CDK4-K38M almost lost the ability to induce zFoxj1a phosphorylation (Fig 6F). These results clearly indicate that Foxj1 can be phosphorylated by CDK4.

We then aimed to determine whether the threonine 102 residue (T102) within the putative conserved substrate motif of zFoxj1a is a major CDK phosphorylation site. Excitingly, we observed that Cyclin D1–CDK4 complexes significantly promoted wild-type zFoxj1a phosphorylation, which was nearly abolished in T102 mutant, an unphosphorylated form of zFoxj1a (Fig 6G). Similarly, in vitro phosphorylation assays showed that purified CDK4 or Cyclin D1–CDK4 complexes resulted in distinct phosphorylation events when incubated with recombinant wild-type zFoxj1a protein but not T102 mutant (Fig 6H). In addition, we observed an increased expression of wild-type zFoxj1a, but not its T102 mutant, in HEK293T cells upon coexpression with CDK4 (Fig 6I). Similarly, CDK4 was able to control mFoxj1 stabilization through phosphorylation of the T87 residue, located in the conserved substrate motif (S11B and S11C Fig). Taken together, we showed that CDK4 directly phosphorylates Foxj1 to suppress its degradation.

zFoxj1a undergoes Ub-independent proteasomal degradation via a direct interaction with Psmd4b

Previous studies have suggested a primary role of the Ub–proteasome system in the elimination of abnormal proteins and selective destruction of regulatory proteins [51, 52]. To explore whether ubiquitination is required for Foxj1 degradation, we examined the effect of Ub K48R/G76A overexpression on zFoxj1a degradation. If zFoxj1a degradation was determined to be

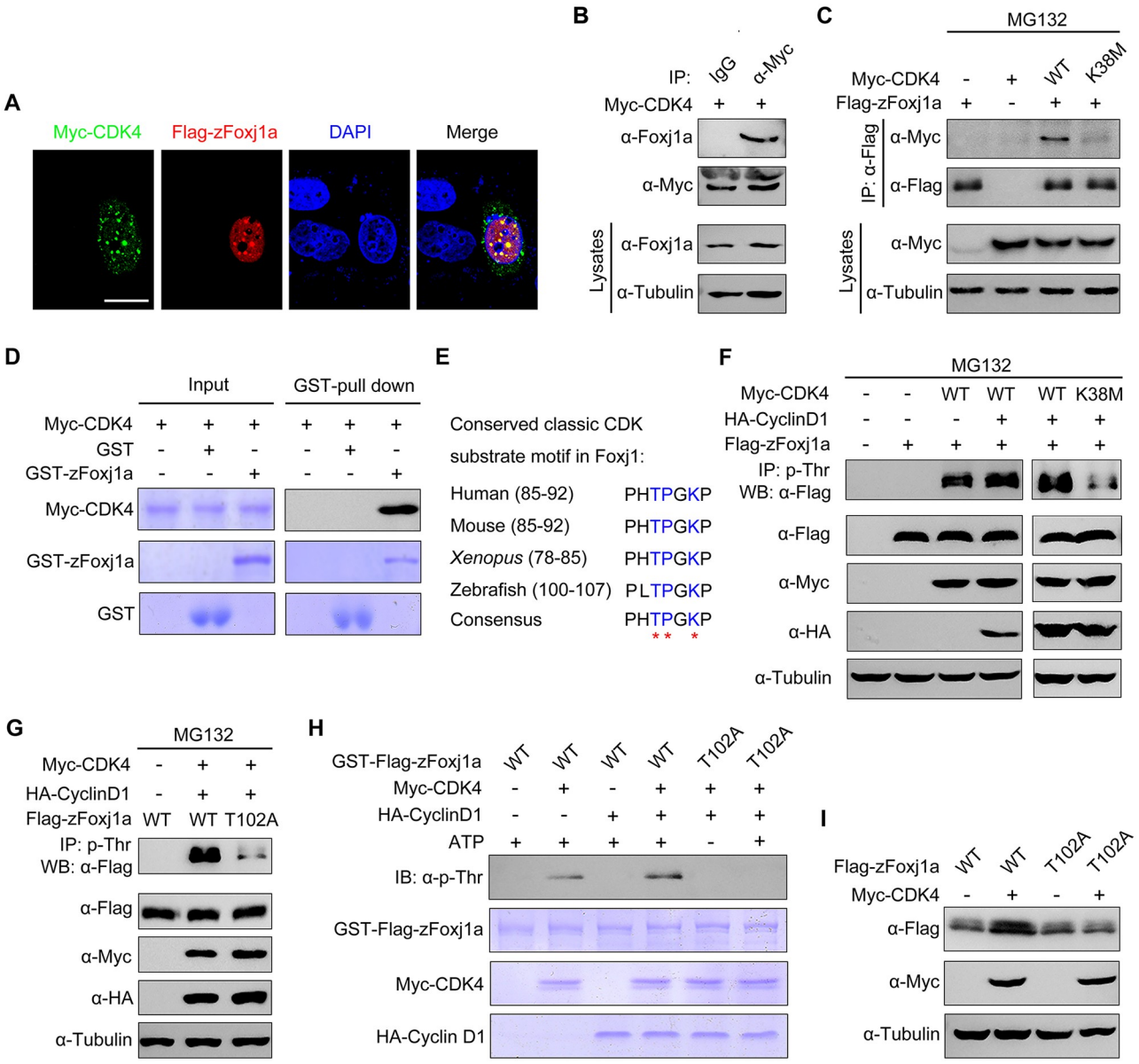

Fig 6. CDK4 phosphorylates zFoxj1a at T102 to suppress its degradation. (A) zFoxj1a and CDK4 show evident colocalization in HeLa cells. HeLa cells were transfected with Flag-zFoxj1a and Myc-CDK4 and immunostained with anti-Flag (red) and anti-Myc (green) antibodies. Nuclei were stained with DAPI (blue). Scale bar, 20 μm. (B) Overexpressed CDK4 interacts with endogenous zFoxj1a. WT embryos were injected with 200 pg Myc-CDK4 mRNA at midgastrulation and then harvested at the bud stage for immunoprecipitation with anti-Myc antibody or normal mouse IgG. (C) CDK4, but not its kinase-deficient mutant, interacts with zFoxj1a. HEK293T cells were transfected with plasmids as indicated, followed by treatment with MG132 for 5 hours prior to harvest for immunoprecipitation. (D) Direct binding of CDK4 to zFoxj1a in vitro. GST, GST-zFoxj1a, and Myc-CDK4 were expressed in bacterial cells and purified. Myc-CDK4 proteins were incubated with GST or GST-zFoxj1a. The presence of Myc-CDK4 in the protein complex pulled down by glutathione agarose was assessed using an anti-Myc antibody. Input proteins were examined by Coomassie blue staining. (E) Conserved CDK substrate motifs in Foxj1 proteins from different species. Red stars indicate critical residues in the CDK substrate motifs. (F–G) CDK4 phosphorylates zFoxj1a at T102. HEK293T cells were transfected with the indicated plasmids. CDK substrates were immunoprecipitated using a phospho-threonine–proline antibody and blotted with anti-Flag antibody to detect phosphorylated zFoxj1a or zFoxj1a-T102A. zFoxj1a-T102A is an unphosphorylated form of zFoxj1a. Note that WT zFoxj1a could be phosphorylated by CDK4 but not by the CDK4-K38M mutant (F). CDK4-mediated phosphorylation was nearly abolished in zFoxj1a-T102A (G). (H) In vitro kinase assays revealed that CDK4 phosphorylates WT zFoxj1a but not the zFoxj1a-T102A mutant. zFoxj1a and zFoxj1a-T102A proteins were purified from bacterial cells and incubated with recombinant Cyclin D1 and CDK4 proteins in the presence or absence of ATP. Phosphorylation of zFoxj1a and zFoxj1a-T102A was detected by western blot using a phospho-threonine–proline antibody, and input proteins were examined by Coomassie blue staining. (I) Ectopic CDK4 expression is unable to stabilize zFoxj1a-T102 mutant. Lysates from HEK293T cells transfected with the indicated plasmids were subjected to immunoblotting. CDK, cyclin-dependent kinase; Foxj1a, forkhead box j1a; GST, glutathione S-transferase; HA, hemagglutinin; HEK, human embryonic kidney; IgG, immunoglobulin G; IP, immunoprecipitation; T102, threonine 102; WB, western blot; WT, wild-type; zFoxj1a, zebrafish Foxj1a; α-Tubulin, acetylated tubulin.

https://doi.org/10.1371/journal.pbio.3000203.g006

ubiquitylation-dependent, we would expect zFoxj1a to be stabilized upon overexpression of Ub K48R/G76A, which serves as a dominant negative inhibitor of poly-Ub chain formation [53, 54]. Indeed, the presence of Ub K48R/G76A, but not wild-type Ub, efficiently inhibited the turnover of β-catenin (S12A Fig), which would be phosphorylated by glycogen synthase kinase-3β and destined for Ub-mediated degradation [55]. Unexpectedly, overexpression of Ub K48R/G76A was unable to promote the stabilization of Flag-tagged zFoxj1a (S12A Fig). Because the Flag epitope contains two lysine residues, we generated a lysine-free version of zFoxj1a, termed HA-zFoxj1a-K20R, by replacing the Flag tag with the HA epitope and mutating all 20 lysine residues within zFoxj1a protein to arginine residues. We found that both the wild-type and lysineless zFoxj1a were significantly stabilized with CDK4 overexpression (S12B Fig). Therefore, zFoxj1a is able to be degraded independently of ubiquitylation.

Increasing evidence suggests that a list of proteins that directly interact with proteasomal subunits are thought to be degraded through a Ub-independent degradation mechanism [56]. It has been demonstrated that the 19S regulatory subunit regulatory particle non-ATPase 10 (Rpn10) plays a critical role in the recognition of Ub-independent substrates [57–59]. Therefore, we examined whether zFoxj1a binds to zebrafish Psmd4b, the ortholog of mammalian Rpn10. Indeed, overexpressed or endogenous zFoxj1a was found to interact with Psmd4b (Fig 7A and 7B). Consistent with these observations, an in vitro binding assay revealed a direct binding between purified zFoxj1a and Psmd4b (Fig 7C).

To further unveil how CDK4 and its kinase activity regulate Foxj1 stabilization, we examined whether CDK4 functions to control the interaction between Psmd4b and zFoxj1a. As expected, ectopic expression of wild-type CDK4, but not its kinase-deficient mutant, dramatically suppressed the association of Psmd4b with zFoxj1a or zFoxj1a-K20R (Fig 7D and 7E). In contrast, the binding ability of the unphosphorylated form of zFoxj1a for Psmd4b was retained with CDK4 coexpression (Fig 7F). Interestingly, the phospho-mimicking mutant of zFoxj1a (zFoxj1a-T102D) completely lost its ability to bind Psmd4b (Fig 7G), suggesting that CDK4-mediated phosphorylation of zFoxj1a at T102 eliminates its affinity for Psmd4b. In addition, Psmd4b overexpression reduced the expression levels of zFoxj1a and its lysine-free mutant (Fig 7H). When HEK293T cells were transfected with same amount of plasmid DNA to express wild-type zFoxj1a and its T102A and T102D mutants, respectively, we detected the highest expression level of zFoxj1a-T102D (Fig 7I). However, T102D mutant could not be further stabilized by CDK4 overexpression (Fig 7I). Taken together, these results indicate that CDK4 phosphorylates and stabilizes zFoxj1a by disrupting its association with Psmd4b.

We next addressed the developmental relevance of CDK4-induced zFoxj1a stabilization. *Cxcr4a*-deficient DFCs exhibited defective *cyclin D1* expression and impaired G1/S transition (Figs 3E–3H and 4F), implying a dysregulated activation of the CDK4/6 kinases. DFC-specific overexpression of zFoxj1a-T102D, but not wild-type or zFoxj1a-T102A, was found to restore the length of KV cilia in *cxcr4a*^{um20} mutants (Fig 7J and 7K). Because zFoxj1a is not involved in DFC proliferation [21, 22], it was reasonable to find that the decrease in the number of cilia was not alleviated (S13 Fig). Overall, our results support a model in which Cxcl12b/Cxcr4a signaling activates ERK1/2, which then promotes Cyclin D1 expression. This, in turn, activates CDK4/6 kinase activity in DFCs. These activated G1 CDKs drive G1/S transition during DFC proliferation and promote zFoxj1a stability by phosphorylation to support KV ciliogenesis at later stages (Fig 7L).

In addition, it is surprising that overexpression of wild-type zFoxj1a could not rescue the length of KV cilia in *cxcr4a*^{um20} mutants because such overexpression should be able to bypass the effects of protein degradation. The FoxP family of transcription factors can bind as homo- or heterodimers, and this interaction is essential for FoxP family members to regulate their targets [60, 61]. These previous observations enlightened us to explore whether Foxj1 proteins

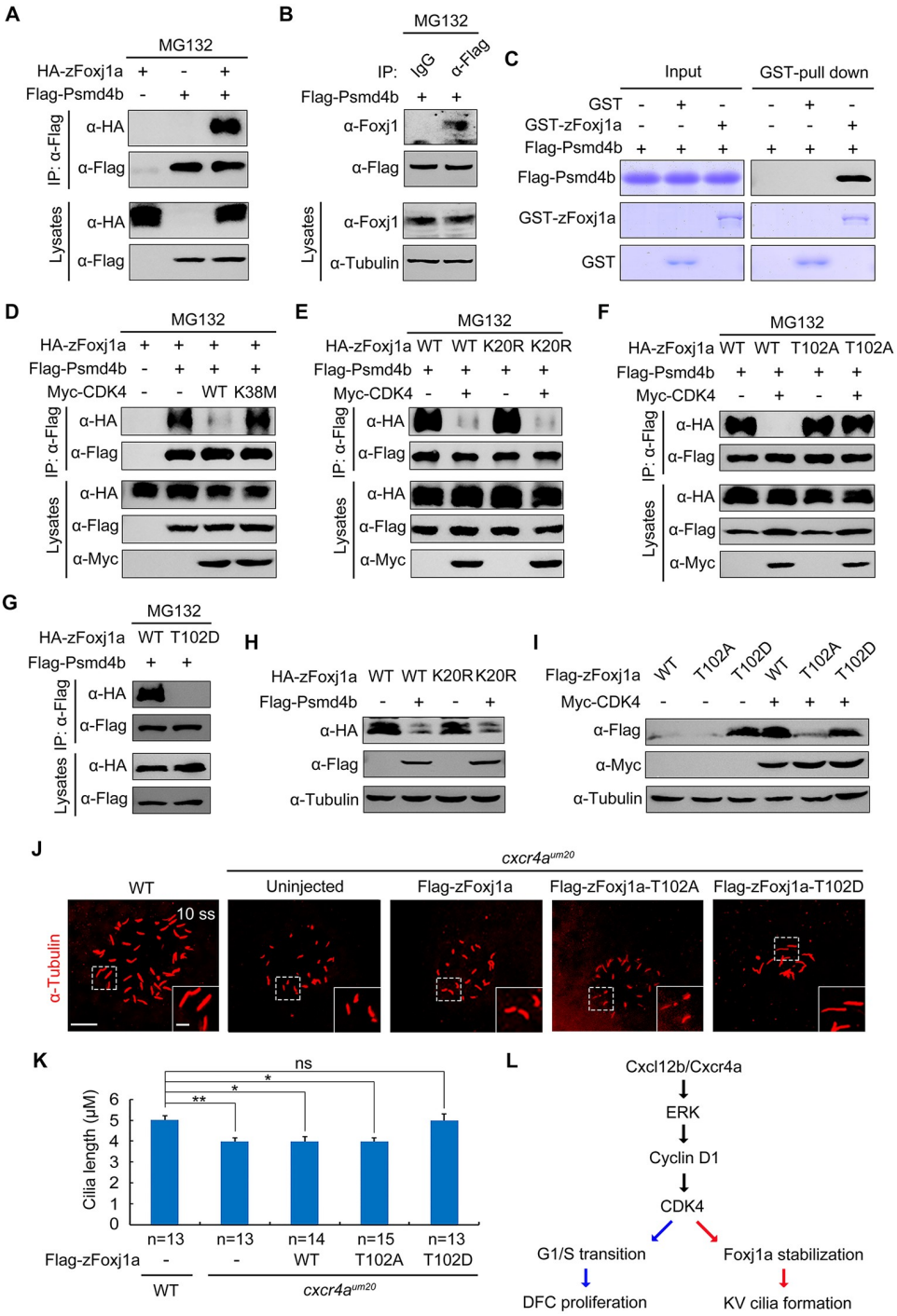

Fig 7. zFoxj1a undergoes Ub-independent proteasomal degradation via a direct interaction with Psmd4b. (A–B) Flag-Psmd4b interacts with overexpressed or endogenous zFoxj1a. HEK293T cells transfected with the indicated constructs (A) and bud-stage WT embryos with DFC-specific expression of Flag-Psmd4b (B) were subjected to immunoprecipitation with the indicated antibodies. (C) In vitro GST pull-down assays reveal a direct interaction between zFoxj1a and Psmd4b. Purified GST or GST-zFoxj1a proteins were incubated with recombinant Flag-Psmd4b. The presence of Flag-Psmd4b in the protein complex that was pulled down by glutathione agarose was assessed by western blot, and input proteins were examined by Coomassie blue staining. (D–E) CDK4 kinase activity is required for its inhibitory effect on the association between Psmd4b and zFoxj1a. HEK293T cells transfected with the indicated plasmids were treated with MG132 for 5 hours prior to harvest for immunoprecipitation. Note that ectopically expressed CDK4 efficiently disrupted the association of Psmd4b with zFoxj1a (D) or its lysine-free mutant zFoxj1a-

K20R (E), while overexpression of the CDK4 kinase-deficient mutant CDK4-K38M had no effect on their interaction (D). (F–G) Psmd4b has a much lower affinity for zFoxj1a-T102D. zFoxj1a-T102A is an unphosphorylated form, and zFoxj1a-T102D is a phospho-mimicking mutant of zFoxj1a. Note that Psmd4b was particularly associated with zFoxj1a and zFoxj1a-T102A (F) but was unable to bind zFoxj1a-T102D (G). The association between Psmd4b and zFoxj1a-T102A was unaffected by CDK4 overexpression (F). (H) Psmd4b overexpression induces a dramatic reduction in zFoxj1a expression. Note that a similar reduction in the expression level of the lysine-free mutant zFoxj1a-K20R was observed upon Psmd4b overexpression. (I) Comparison of protein stability in WT zFoxj1a and its mutants. HEK293T cells were transfected with the indicated constructs and harvested for western blot analysis. In comparison to WT zFoxj1a and its T102A mutant, the zFoxj1a-T102D mutant exhibited greater stability but could not be further stabilized by CDK4 overexpression. (J–K) DFC-specific overexpression of zFoxj1a-T102D in *cxcr4a*^{um20} mutants restores KV cilia length. Confocal images of 10-somite–stage *cxcr4a*-deficient embryos were injected with 200 pg of WT *zfoxj1a* or *zfoxj1a-T102A* or *zfoxj1a-T102D* mRNA at the 256-cell stage. The resulting embryos were harvested at the 10-somite stage for immunostaining using an antibody against α-Tubulin (J). The boxed areas in the images are presented at higher magnification in the relevant insets. Scale bar, 20 μm. Statistical data for cilia length are shown in panel K. Student *t* test, $^{*}P < 0.05$, $^{**}P < 0.01$. Underlying data can be found in S1 Data. (L) A schematic diagram showing the regulatory mechanism of Cxcl12/Cxcr4a signaling in DFC proliferation and cilia formation. CDK, cyclin-dependent kinase; DFC, dorsal forerunner cell; ERK, extracellular regulated MAP kinase; Fox1ja, forkhead box j1a; GST, glutathione S-transferase; HA, hemagglutinin; HEK, human embryonic kidney; IgG, immunoglobulin G; IP, immunoprecipitation; KV, Kupffer's vesicle; ns, no significant difference; Psmd4b, proteasome 26S subunit, non-ATPase 4b; T102, threonine 102; Ub, ubiquitin; WT, wild-type; zFoxj1a, zebrafish Foxj1a; α-Tubulin, acetylated tubulin.

https://doi.org/10.1371/journal.pbio.3000203.g007

exist as a dimer. To test this, HEK293T cells were transfected with plasmids expressing Flag-zFoxj1a and HA-zFoxj1a. Coimmunoprecipitation experiments revealed a physical interaction between zFoxj1a proteins tagged with different epitopes (S14A and S14B Fig). Interestingly, compared with wild-type proteins, the unphosphorylated form of zFoxj1a showed a much-reduced affinity to each other, while the phospho-mimicking mutants exhibited a stronger binding ability to form complexes (S14C Fig). Moreover, whole-cell lysates containing overexpressed Flag-tagged wild-type zFoxj1a or its T102A or T102D mutants were separated on SDS- and native PAGEs, respectively. Most of the wild-type as well as the phospho-mimicking proteins gave rise to a band about 130 kD, corresponding to zFoxj1a dimers in native PAGEs, implying that the wild-type zFoxj1a proteins might be phosphorylated at T102 to avoid degradation and form homodimers (S14D Fig). Indeed, the dimerization of the unphosphorylated zFoxj1a mutants was obviously decreased (S14D Fig). These results implicate that the phosphorylation at T102 site of zFoxj1a is important for its dimerization. Based on these observations, we supposed that the insufficiency of Cyclin D1–CDK4/6 activity in *cxcr4a*^{um20} mutants would lead to impaired dimerization of overexpressed wild-type zFoxj1a proteins, which might eventually deprive them of their transcriptional activity.

Discussion

In zebrafish embryos, DFCs undergo mitotic proliferation during epiboly and then exit the cell cycle, giving rise to epithelial cells that assemble cilia in the mature KV organ [16]. Cell-cycle defects in DFCs are often accompanied by an alteration in KV cilia elongation, raising the issue of whether there exists a feasible link between the cell cycle and cilia formation [16–18]. In this study, our experiments resolve this issue by demonstrating that Cxcr4 signaling is required for DFC proliferation and KV ciliogenesis by promoting Cyclin D1 expression. Specifically, we found that Cyclin D1–CDK4/6 accelerates the G1/S transition in DFCs while also facilitating cilia formation via stabilization of zFoxj1a. Ciliary dynamics appear to be precisely coordinated with cell-cycle progression [62]. It has been suggested previously that cell quiescence is essential for the formation of mouse nodal cilia [63]. Indeed, we observed that proliferating DFCs enter into a quiescent state upon differentiation into ciliated epithelial KV cells. Interestingly, our data indicate that during epiboly stages, Cxcr4a-signal–induced expression of Cyclin D1 functions to regulate DFC proliferation and zFoxj1a stability, which is important

for the ciliogenesis of quiescent KV cells. Therefore, the rapid cell-cycle progression of DFCs during epiboly stages is not only required for the generation of enough cells to construct KV but also plays a critical role in reserving sufficient levels of zFoxj1a protein to support subsequent cilia formation. Because Wnt/β-catenin signaling has been reported to play a role in both DFC proliferation and KV cilia elongation [17, 18], it is interesting to consider whether this signaling pathway contributes to zFoxj1a stabilization via regulation of cell-cycle progression during the establishment of L–R asymmetry.

Most *cxcr4a* or *cxcl12b* mutants display a severe KV morphogenesis phenotype, a reduction in cilia length, and abnormal fluid flow in KV, but these embryos exhibit a relatively low penetrance in the situs abnormalities at later stages. Moreover, the mutated Cxcr4a has no residual activity because of its inability to rescue the laterality defects in *cxcr4a*^{um20} embryos. It has been well established that the Nodal–Pitx2 pathway (the Spaw–Pitx2c pathway in zebrafish) plays a central and conserved role in L–R symmetry breaking [1]. Recently, a zebrafish mutant defective for the *spaw* gene has been identified [64]. Surprisingly, in 70% of the *spaw* mutant embryos, cardiac looping occurs in the correct dextral direction. That is to say, only about 30% of the *spaw* mutants showed a "no-looping" or reversed "left-looping" heart [64]. This previous study proposed a Nodal- and KV-function–independent mechanism that drives asymmetric heart looping in zebrafish embryos [64]. In our study, about 20% of the *cxcr4a* or *cxcl12b* mutants showed a "no-looping" or reversed "left-looping" heart, which is slightly lower than that of *spaw* mutants. Therefore, Cxcr4a signaling primarily functions in regulating KV formation and ciliogenesis but may have little role in fulfilling the Nodal- and KV-function–independent mechanism. In addition, a higher percentage of *spaw* mutants (about 50%) exhibited the L–R asymmetry defects in digestive system laterality [64]. However, a relative lower percentage of *cxcr4a* or *cxcl12b* mutants (about 30%) displayed liver laterality defects. Similarly, it has been reported that *cxcr4a*^{um20} mutants showed a partial penetrance of circulation defects by day 2 of development [34]. These observations suggest that there could be some unknown mechanisms to partially compensate for the function of *cxcr4a* at later developmental stages.

It has been reported previously that G1 cyclins function together with their associated CDKs to phosphorylate a variety of transcription factors, including Smad2/3 and pluripotency factors, to control ES cell differentiation [11, 12]. A systematic screen for CDK4/6 substrates identified fox family transcription factor forkhead box M1 (FOXM1) as a critical phosphorylation target [65]. CDK4/6 stabilize and activate FOXM1 by phosphorylation at multiple sites to protect cancer cells from senescence [65]. In contrast, CDK2 reduces DNA-damage–induced cell death by phosphorylation of forkhead box O1 (FOXO1) at Ser249, resulting in cytoplasmic localization of FOXO1 [66]. In this study, we show that CDK4 directly interacts with and phosphorylates zFoxj1a at a conserved "TPGK" motif within the N-terminal region. Phosphorylation at T102 was not found to alter the subcellular distribution of zFoxj1a but was shown to promote its stabilization. Therefore, the functional interaction between CDK4 and zFoxj1a provides a mechanism by which cilia development is facilitated. Because CDK4 also stabilizes mFoxj1 through phosphorylation of T87 within the substrate motif, it is likely that the molecular linkage between cell-cycle progression and ciliogenesis is conserved among vertebrates.

Previous studies have shown that individual knockout of either *Cdk4* or *Cdk6* in mice did not reveal any obvious developmental defects [67, 68]. In contrast, embryos defective for *Cdk4* and *Cdk6* die during the late stages of embryonic development because of severe anemia [68]. *Cdk2* knockout mice were viable and developed normally [69]. However, compound mutation of *Cdk4* and *Cdk2* results in impaired proliferation and heart growth [70]. These results indicate a putative redundant or compensatory role of these G1 phase *Cdk* genes. The complicated interactions between these *Cdk* genes also prevent us from exploring the in vivo functions of zebrafish *cdk4* in DFCs or KV cells. Nevertheless, we found that wild-type embryos treated

with the CDK4/6 chemical inhibitor PD0332991 exhibited L–R defects. Moreover, overexpression of Cyclin D1 in *cxcr4a* mutants ideally rescued the defects in KV cell proliferation and cilia formation. These observations suggest an important function of CDK4/6 in connecting cell-cycle progression with cilia formation.

The majority of proteosomal protein degradation relies on Ub conjugation. However, there are increasing numbers of examples of proteasomal degradation that occur without prior ubiquitination [71, 72]. Our study reveals that overexpression of the dominant negative Ub has no effect on zFoxj1a stabilization. However, wild-type and lysineless zFoxj1a are found to be similarly stabilized by ectopic CDK4 expression. Therefore, zFoxj1a is targeted for proteasomal degradation in a Ub-independent manner. Intriguingly, E3 Ub ligases, including mahogunin RING finger 1 (MGRN1) and Lnx2b, have been reported to play a role in L–R laterality specification in rodents and zebrafish [24, 73], suggesting a role of the Ub–proteasome system in the modulation of protein turnover during L–R body patterning. However, because of the fact that L–R symmetry breaking occurs within a short time window during vertebrate embryonic development [4, 74], the accelerated and economical regulation of protein degradation may be essential. Because Ub-independent degradation does not require the enzymatic cascade of Ub conjugation, it would be more efficient to alter the concentration of zFoxj1a protein levels via Ub-independent proteasomal degradation during L–R asymmetric development. Interestingly, a recent study has demonstrated that Foxj1 is rapidly turned over by the Ub–proteasome system in mouse primary ependymal cells [75]. Therefore, Foxj1 is a protein with a short half-life that undergoes proteasomal degradation via Ub-dependent or independent pathways dependent on the cellular context.

Several proteins have been reported to interact with the 19S regulatory subunit Rpn10 via their Ub-like (UBL) domains [57–59]. Interestingly, while lacking a UBL domain, zFoxj1a interacts directly with Psmd4b, the zebrafish ortholog of mammalian Rpn10. Our study demonstrates that CDK4 phosphorylates and stabilizes zFoxj1a by disrupting its association with Psmd4b. Similarly, the Ub-independent proteasomal degradation of Yeast phosphatidic acid phosphohydrolase 1 (Pah1) has also shown to be governed by its phosphorylation state [76]. Therefore, this may represent a general mechanism by which protein kinase-mediated phosphorylation plays a critical role in the protection of their substrates from Ub-independent proteasomal degradation.

Materials and methods

Ethics statement

Our zebrafish experiments were all approved and carried out in accordance with the Animal Care Committee at the Institute of Zoology, Chinese Academy of Sciences (permission number: IOZ-13048).

Zebrafish strains

Wild-type embryos were obtained from natural matings of Tübingen zebrafish. Embryos were raised in Holtfreter's solution at 28.5 ˚C and staged by morphology. Homozygous *cxcr4a*^{um20} mutants were identified from the offspring of heterozygous *cxcr4a*^{um20} parents through genotyping as previously described [34]. Primers for genotyping were *cxcr4a* FWD1, 5′-CCAACT TTGAGGTCCCGTGTGATG-3′, and *cxcr4a* REV1, 5′-CTGTGGACACGGATGACATTC CTG-3′. PCR products were digested using DdeI. *cxcl12b*^{mu100} embryos were obtained by incrossing homozygous male and female *cxcl12b*^{mu100} adult mutants carrying loss-of-function alleles of the *cxcl12b* gene [38]. *Tg(sox17:GFP)* transgenic embryos were used to indicate the DFCs and KV cells during L–R asymmetric development. *Tg(EF1α:mKO2-zCdt1(1/190))*

transgenic embryos express the fluorescent fusion protein mKO2-zCdt1(1/190) in cells at the G1 phase during embryonic development. *Tg(flk:EGFP)* transgenic embryos express EGFP in blood vessels.

RNA synthesis, MOs, and microinjection

Capped mRNAs for *cxcr4a*, *caMEK1*, *cyclin D1*, *zfoxj1a*, *zfoxj1a-T102A*, and *zfoxj1a-T102D* were synthesized in vitro from corresponding linearized plasmids using the mMessage mMachine kit (Ambion, Austin, TX, USA). Digoxigenin-UTP–labeled antisense RNA probes were in vitro transcribed using the MEGAscript Kit (Ambion) according to the manufacturer's instructions. The standard cMO (5′-CCTCTTACCTCAGTTACAATTTATA-3′), splicing MO targeting *cxcr4a* (5′-AGACGATGTGTTCGTAATAAGCCAT-3′), and MO targeting the start codon of *foxj1a* (5′-CATGGAGAGCATGGTCCTGACAAAT-3′) were purchased from Gene Tools (Philomath, OR, USA) and used as previously described [21, 31, 77]. For DFC-specific knockdown or overexpression experiments, indicated MOs or mRNAs were injected into the yolk at the 256-cell stage as described previously [37].

WISH

WISH was performed using the NBT-BCIP substrate following standard procedures. For two-color fluorescence in situ hybridization, anti-digoxigenin-POD (11633716001; Roche, Basel, Switzerland) and anti-fluorescein-POD (11426346910, Roche) were used as primary antibodies to detect digoxigenin-labeled sox17 probes and fluorescein-labeled *cyclin D1* probes, respectively. Fluorescence in situ hybridization was then carried out using the Perkin Elmer TSA fluorescein system (NEL701A001KT; Waltham, MA, USA) according to the manufacturer's instructions.

Cell lines and transfection

HEK293T and HeLa cell lines (American Tissue Culture Collection [ATCC], Manassas, VA, USA) were cultured in DMEM medium supplemented with 10% FBS in a 37 ˚C humidified incubator in a 5% CO_2 environment. Cell transfections were carried out using Lipofectamine 2000 (11668019; Invitrogen, Carlsbad, CA, USA) following the manufacturer's instructions.

Immunostaining and confocal microscope

Embryos were fixed in 4% paraformaldehyde overnight. Fixed embryos were then rinsed with PBST for a total of 4 times every 5 minutes. Embryos were then blocked at room temperature for 1 hour in 10% heat-inactivated goat serum and then stained with the following affinity-purified primary antibodies overnight at 4 ˚C: anti-β-catenin antibody (1:500; ab6302, Abcam, Cambridge, UK), anti-Cdh1 (1:200; GTX125890, GeneTex, Irvine, CA, USA), anti-pERK1/2 (1:1,000; 9101, Cell Signaling Technology, Danvers, MA, USA), anti-α-Tubulin antibody (1:400; T6793, Sigma-Aldrich, St. Louis, MO, USA), anti-α-PKC (1:200, sc-216, Santa Cruz Biotechnology, Santa Cruz, CA, USA), anti-GFP (1:1,000; A-11122, Invitrogen), anti-GFP (1:1,000; A-11120, Invitrogen), and anti-Foxj1 (1:200; ab220028, Abcam). Samples were then washed 3 times with PBST, followed by incubation with secondary antibodies, including DyLight 488-conjugated goat anti-rabbit IgG (1:200; 711-545-152, Jackson ImmunoResearch, West Grove, PA, USA), DyLight 594-conjugated goat anti-mouse IgG (1:200; 715-585-150, Jackson), DyLight 488-conjugated AffiniPure goat anti-mouse IgG (1:200; 715-545-150, Jackson), and DyLight 594-conjugated AffiniPure goat anti-rabbit IgG (1:200; 711-585-152, Jackson), for 1 hour at room temperature. In some experiments, DAPI (1:10,000, Sigma-Aldrich)

was used to stain nuclei. The stained embryos were then embedded with 2% low melting agarose and imaged using a Nikon A1R+ confocal microscope (Nikon, Tokyo, Japan) with identical settings.

Pharmacological treatment

To block CDK activity, embryos were treated with 0.5 μM PD0332991 (A8318, Selleckchem, Houston, TX, USA) or 0.2 μM CYC202 (A1723, Selleckchem) from the shield stage to the bud stage. For CDK4/6 inhibition in cultured cells, HEK293T cells were treated with 0.5 μM PD0332991 for 5 hours prior to harvest. In order to examine which pathway is required for zFoxj1a degradation, HEK293T cells were transfected with plasmids expressing Flag-zFoxj1a and treated with 20 mM NH_4Cl (A116363, Aladdin, Shanghai, China), 20 μM MG132 (M7449, Sigma-Aldrich), and 5 mM 3-MA (M9281, Sigma-Aldrich), respectively, for 5 hours prior to harvest.

Fluorescent bead tracking

Fluorescent red beads of 1 uM diameter (1:500; 18660–5, Polysciences, Warrington, PA, USA) were injected into KV of embryos at the 6-somite stage. The resulting embryos were then embedded in 2% low-melting agarose at the 10-somite stage for confocal imaging. Beads tracking videos and images were processed using Image Pro 6.0.

High-speed cilia video microscopy

For recording cilia motility in KV, we embedded 10-somite–stage embryos in 3% methylcellulose on glass cover slides. Cilia movements were recorded with a high-speed camera (MotionBLITZ EoSens mini1; Mikrotron, Unterschleiβheim, Germany) mounted on a Leica Sp8 confocal microscope with a 100× oil objective in bright field. Movies were recorded at a rate of 500 frames per second, and playbacks were at 25 frames per second.

Antibodies and immunoprecipitation assays

For immunoblotting experiments, we used the following affinity-purified antibodies: anti-Flag (1:5,000; F2555, Sigma-Aldrich), anti-Myc (1:3,000; M047-3, MBL Medical & Biological Laboratories, Nagoya, Japan), anti-HA (1:3,000; CW0092A, CWBIO, Beijing, China), anti-β-Tubulin (1:5,000, CW0098M, CWBIO), and anti-Foxj1 (1:200; ab220028, Abcam).

For coimmunoprecipitation assays, embryos or HEK293T cells were harvested and lysed with TNE lysis buffer (10mM Tris-HCl [pH 7.5], 150 mM NaCl, 2 mM EDTA, and 0.5% Nonidet P-40) containing a protease inhibitor mixture. Lysates were incubated with anti-Flag-agarose beads (A2220, Sigma-Aldrich) or protein A-Sepharose beads (101041, Invitrogen) and anti-phospho-threonine–proline antibody (1:5,000; 9391, Cell Signaling Technologies) at 4 ˚C for 4 hours. Beads were washed 4 times with TNE buffer. Bound proteins were then separated by SDS-PAGE and visualized by western blots.

BrdU incorporation assay

Half an hour before the embryos were fixed for BrdU labeling experiments, they were dechorionated and incubated with 10 mM BrdU solution (B5002, Sigma-Aldrich) for 20 min at 4 ˚C. Then, these embryos were allowed to develop to desired stages in Holtfreter's solution at 28.5 ˚C. Incorporated BrdUs and GFP were detected using anti-BrdU (1:1,000; ab6326, Abcam) and rabbit anti-GFP antibodies (1:1,000; A-11122, Invitrogen) by whole-mount immunostaining.

In vitro GST pull-down

GST fusion proteins were expressed in *Escherichia coli* strain BL21 and purified using Glutathione-Sepharose 4B beads (71024800-GE, GE Healthcare, Chicago, IL, USA). GST-Myc-CDK4, GST-HA-cyclinD1, and GST-Flag-psmd4b were treated with Thrombin (1:1,000; T4648, Sigma-Aldrich) to cleave their GST tags. For in vitro binding assays, GST-Foxj1a proteins were immobilized by Glutathione-Sepharose 4B beads and incubated with the indicated purified proteins at 4 ˚C for 3 hours. Following washing, the bound proteins were separated with SDS-PAGE and analyzed by western blots.

In vitro kinase assay

For in vitro kinase assays, 1 μg GST-Foxj1a or GST-Foxj1a-T102A was incubated with 1 μg of the indicated purified proteins in 1× kinase buffer (25 mM Tris-Cl [pH7.5], 5 mM β-glycerophosphate, 0.1 mM Na_3VO_4, 10 mM $MgCl_2$, 2 mM dithiothreitol) with or without 50 μM ATP (P0756S, New England Biolabs, Ipswich, MA, USA) at 30 ˚C for 30 min. The mixture was then separated on 10% SDS-PAGE and visualized by western blots or Coomassie blue staining.

Statistical analysis

Cilia number and length were measured using ImageJ software. All results were expressed as the mean ± SD. Differences between control and treated groups were analyzed using the unpaired two-tailed Student *t* test. Results were considered statistically significant at $P < 0.05$.

Supporting information

S1 Fig. The expression of *cxcr4a* in DFCs and KV cells. (A) *cxcr4a* expression during gastrulation. In situ hybridization of *cxcr4a* in embryos at the 75% epiboly stage (dorsal view with animal pole to the top) and bud stage (lateral views with animal pole to the top). Black arrowhead indicates the DFCs. (B) *cxcr4a* expression at the 6-somite stage. Lateral view was shown with animal pole to the top in the left panel, and dorsal view was shown in the right panel. Black arrowhead indicates the KV. (C) Confocal images depicting the formation of the lateral dorsal aorta in live *Tg(flk:GFP)* embryos. Scale bar, 50 μm. DFC, dorsal forerunner cell; ep, epiboly; *flk*, *fms-like tyrosine kinase*; GFP, green fluorescent protein; KV, Kupffer's vesicle; LDA, lateral dorsal aorta; PHBC, primordial hindbrain channel; Tg, transgene.
(TIF)

S2 Fig. Overexpression of Cxcr4a^{um20} has no rescue effect on the laterality defects in *cxcr4a*-defective embryos. (A–B) Embryo ratios with different expression patterns of *cmlc2* (A) and *hhex* (B) at 48 hpf in *cxcr4a*^{um20} mutants injected with 300 pg *cxcr4a* or *cxcr4a*^{um20} mRNA at the 256-cell stage. Underlying data can be found in S1 Data. *cmlc2*, cardiac myosin light chain 2; *hhex*, hematopoietically expressed homeobox; hpf, hours postfertilization.
(TIF)

S3 Fig. The zygotic, but not maternal, *cxcr4a* function is required for L–R asymmetric development. (A–B) The percentage of embryos with different phenotypes in cardiac looping (A) and liver laterality (B). The maternal *cxcr4a* mutants (M*cxcr4a*) were generated by crossing MZ*cxcr4a* mutant adult females with wild-type male fish. Underlying data can be found in S1 Data. (C–D) Analysis of cardiac looping (C) and liver laterality (D) in wild-type (*cxcr4a*$^{+/+}$) embryos and zygotic *cxcr4a*^{um20} heterozygous (*cxcr4a*$^{-/+}$) or homozygous (*cxcr4a*$^{-/-}$) mutants. *cxcr4a*$^{-/+}$ and *cxcr4a*$^{-/-}$ embryos were identified from *cxcr4a*^{um20} heterozygous fish crosses by

genotyping. Underlying data can be found in S1 Data. L–R, left–right.
(TIF)

S4 Fig. *cxcr4a* is unnecessary for the specification, clustering, and collective migration of DFCs and dispensable for the polarized differentiation of KV cells. (A) Time-lapse confocal images showing DFC migration in wild-type and *cxcr4a*^{um20} mutant embryos on a *Tg(sox17:GFP)* background from 75%–90% epiboly stages. Scale bar, 50 μm. (B) Sox17 expression was examined by in situ hybridization in wild-type and *cxcr4a*^{um20} mutants at the 75% epiboly stage. (C–D) Wild-type and *cxcr4a*-deficient *Tg(sox17:GFP)* embryos were harvested at the 10-somite stage for immunostaining. KV cells were labeled using an antibody against GFP. Expression of the basal–lateral marker E-cadherin (C) and the apical marker aPKC (D) were visualized using the indicated antibodies. Scale bar, 20 μm. aPKC, atypical protein kinase; DFC, dorsal forerunner cell; GFP, green fluorescent protein; KV, Kupffer's vesicle; *sox*, SRY-box transcription factor; Tg, transgene.
(TIF)

S5 Fig. Deficiency of *cxcl12b* results in severe defects in KV ciliogenesis. Wild-type embryos and *cxcl12b*^{mu100} mutants were harvested at the 10-somite stage for fluorescent immunostaining using anti-α-Tubulin antibody (A). Scale bar, 20 μm. Cilia average number and length were quantified from three independent experiments, and the group values were expressed as the mean ± SD (B and C). Student *t* test, $^{*}P < 0.05$, $^{**}P < 0.01$. Underlying data can be found in S1 Data. KV, Kupffer's vesicle; α-Tubulin, acetylated tubulin.
(TIF)

S6 Fig. KV cells of *cxcr4a* morphants exhibit impaired G1/S transition. *Tg(sox17:GFP;EF1α:mKO2-zCdt1(1/190))* embryos were injected with 8 ng cMO or *cxcr4a* MO at the 256-cell stage, and then harvested at the indicated developmental stages for in vivo confocal imaging (A and C). Scale bar, 20 μm. The percentage of mKO2-positive KV cells were quantified from three independent experiments (B and D). The significance of differences compared with the control group were analyzed with the Student *t* test, $^{***}P < 0.001$. Underlying data can be found in S1 Data. cMO, control MO; EF1α, eukaryotic translation elongation factor 1α; GFP, green fluorescent protein; KV, Kupffer's vesicle; mKO2, monomeric Kusabira Orange2; MO, morpholino; *sox*, SRY-box transcription factor; Tg, transgene; zCdt1, zebrafish chromatin licensing and DNA replication factor 1.
(TIF)

S7 Fig. *cxcr4a*^{um20} mutants exhibit a normal expression of *foxj1a* transcripts. *foxj1a* expression was examined by in situ hybridization at the 75% epiboly and bud stages in wild-type and *cxcr4a*^{um20} mutant embryos. Foxj1a, forkhead box j1a.
(TIF)

S8 Fig. Validation of the specificity of an antibody against human FOXJ1 in *foxj1a* morphants. (A) Wild-type embryos were injected with 3 ng cMO or z*foxj1a* MO at the one-cell stage and harvested for western blotting at the 75% epiboly stage. (B and C) Detection of zFoxj1a protein in the floor plate of the spinal cord and pronephric duct. cMO- and z*foxj1a* MO-injected embryos at 24 hpf were stained with anti-FOXJ1 antibody and DAPI. The floor plate of the spinal cord (B) and pronephric duct (C) were observed after immunostaining. Note that the expression of zFoxj1a protein was significantly decreased in *foxj1a* morphants. Scale bar, 50 μm. cMO, control MO; Foxj1a, forkhead box j1a; hpf, hours postfertilization; MO, morpholino; zFoxj1a, zebrafish Foxj1a.
(TIF)

S9 Fig. Inactivity of *cxcr4a* does not affect β-catenin nuclear accumulation in DFCs. Wild-type and *cxcr4a*^{um20} mutants were harvested at the 75% epiboly stage for immunofluorescence assays using the indicated antibodies. Scale bar, 20 μm. DFC, dorsal forerunner cell.
(TIF)

S10 Fig. Validation of the efficiency of CDK chemical inhibitors in live embryos. *Tg(mKO2-zCdt1(1/190))* embryos were treated with 0.5 μM PD0332991 or 0.2 μM CYC202 from the shield stage to the 10-somite stage. Then, these embryos were harvested for in vivo confocal imaging. Note that both PD0332991 and CYC202 treatments induced a remarkable increase of the number of mKO2-zCdt1–positive cells. Scale bar, 200 μm. CDK, cyclin-dependent kinase; EF1α, eukaryotic translation elongation factor 1α; mKO2, monomeric Kusabira Orange2; Tg, transgene; zCdt1, zebrafish chromatin licensing and DNA replication factor 1.
(TIF)

S11 Fig. CDK4 phosphorylates and stabilizes mFoxj1. (A–B) HEK293T cells were transfected with the indicated plasmids and then harvested for immunoprecipitation with a phospho-threonine–proline antibody. Phosphorylation of mFoxj1 (A) and its T87A mutant (B) was detected by western blot. Note that the CDK4-mediated phosphorylation of mFoxj1 was clearly decreased in the T87A mutant. (C) Western blots of total lysates from HEK293T cells transfected with the indicated plasmids. Note that CDK4 overexpression could stabilizes wild-type mFoxj1 but not the T87A mutant. CDK, cyclin-dependent kinase; HEK, human embryonic kidney; Foxj1, forkhead box j1a; mFoxj1, mouse Foxj1.
(TIF)

S12 Fig. Proteasomal degradation of zFoxj1a is independent of Ub modification. (A) Overexpression of Ub K48R/G76A was unable to stabilize zFoxj1a. Flag-tagged β-catenin and zFoxj1a were coexpressed with wild-type Ub or Ub K48R/G76A, a dominant negative inhibitor of chain formation and degradation. Cell extracts were immunoblotted with the indicated antibodies. (B) CDK4 overexpression similarly promoted the expression of wild-type zFoxj1a and its lysineless mutant K20R. CDK, cyclin-dependent kinase; Foxj1a, forkhead box j1a; Ub, ubiquitin; zFoxj1a, zebrafish Foxj1a.
(TIF)

S13 Fig. The decrease in the number of cilia in *cxcr4a*^{um20} mutants was not alleviated by DFC-specific overexpression of wild-type zFoxj1a and its T102A and T102D mutants, respectively. *cxcr4a*-deficient embryos were injected with 200 pg of wild-type *zfoxj1a* or *zfoxj1a-T102A* or *zfoxj1a-T102D* mRNA at the 256-cell stage. The resulting embryos were harvested at the 10-somite stage for immunostaining using an antibody against α-Tubulin. Cilia number was quantitatively analyzed using ImageJ software. Student *t* test, $^{**}P < 0.01$. Underlying data can be found in S1 Data. DFC, dorsal forerunner cell; Foxj1a, forkhead box j1a; ns, no significant difference; T102, threonine 102; zFoxj1a, zebrafish Foxj1a; α-Tubulin, acetylated tubulin.
(TIF)

S14 Fig. Phosphorylation of T102 is essential for the dimerization of zFoxj1a proteins. (A–C) In vivo self-association of zFoxj1a. HEK293T cells were transfected with indicated plasmids encoding differently tagged wild-type zFoxj1a or its mutants. Lysates were immunoprecipitated with anti-Flag or anti-HA antibodies and then immunoblotted with indicated antibodies. In panel C, HEK293T cells were treated with MG132 for 5 hours prior to harvest for immunoprecipitation. (D) zFoxj1a forms homodimers. HEK293T cells were transfected with indicated plasmids encoding Flag-tagged wild-type zFoxj1a or its mutants. Lysates were then separated

on SDS- and native PAGEs, respectively. Foxj1a, forkhead box j1a; HA, hemagglutinin; HEK, human embryonic kidney; T102, threonine 102; zFoxj1a, zebrafish Foxj1a.
(TIF)

S1 Raw Images. The uncropped blots for the westerns and immunoprecipitations.
(PDF)

S1 Movie. Wild-type embryos, normal KV flow. Wild-type *Tg(sox17:GFP)* embryos were injected at the 6-somite stage with fluorescent beads and imaged using a Nikon A1R+ confocal microscope at the 10-somite stage. Dorsal view with anterior to the top. GFP, green fluorescent protein; KV, Kupffer's vesicle; *sox*, SRY-box transcription factor; Tg, transgene.
(MP4)

S2 Movie. *cxcr4a*^{um20} mutant embryos, aberrant KV flow. *cxcr4a*^{um20} mutant embryos on a *Tg(sox17:GFP)* background were injected at the 6-somite stage with fluorescent beads and imaged using a Nikon A1R+ confocal microscope at the 10-somite stage. Dorsal view with anterior to the top. GFP, green fluorescent protein; KV, Kupffer's vesicle; sox, SRY-box transcription factor; Tg, transgene.
(MP4)

S3 Movie. The beating cilia of KV cells in wild-type embryos. Wild-type embryos were imaged using a high-speed video microscopy at the 10-somite stage. Dorsal view with anterior to the top. KV, Kupffer's vesicle.
(MP4)

S4 Movie. The beating cilia of KV cells in *cxcr4a*^{um20} mutants. *cxcr4a*^{um20} mutant embryos were imaged using a high-speed video microscopy at the 10-somite stage. Dorsal view with anterior to the top. KV, Kupffer's vesicle.
(MP4)

S1 Data. Numerical data used in Figs 1, 2, 3, 4, 5 and 7, S2, S3, S5, S6 and S13 Figs.
(XLSX)

Acknowledgments

We are grateful to Dr. Jingwei Xiong (Peking University, China) for the *Tg(EF1α:mKO2-zCdt1(1/190))* fish line and Dr. Linfei Luo (Southwest University, China) for *cxcr4a*^{um20} and *cxcl12b*^{mu100} fish lines. We also thank Dr. Chengtian Zhao (Ocean University of China, China) for help with the measurement of cilia motility by high-speed video microscopy.

Author Contributions

Conceptualization: Sizhou Huang, Qiang Wang.

Data curation: Qiang Wang.

Formal analysis: Sizhou Huang.

Investigation: Jingwen Liu, Chengke Zhu, Guozhu Ning, Liping Yang, Yu Cao.

Project administration: Qiang Wang.

Validation: Qiang Wang.

Visualization: Qiang Wang.

Writing – original draft: Jingwen Liu.

Writing – review & editing: Qiang Wang.

References

1. Grimes DT, Burdine RD. Left-Right Patterning: Breaking Symmetry to Asymmetric Morphogenesis. Trends in genetics: TIG. 2017; 33(9):616–28. https://doi.org/10.1016/j.tig.2017.06.004 PMID: 28720483
2. Essner JJ, Amack JD, Nyholm MK, Harris EB, Yost HJ. Kupffer's vesicle is a ciliated organ of asymmetry in the zebrafish embryo that initiates left-right development of the brain, heart and gut. Development. 2005; 132(6):1247–60. https://doi.org/10.1242/dev.01663 PMID: 15716348.
3. Hirokawa N, Tanaka Y, Okada Y, Takeda S. Nodal flow and the generation of left-right asymmetry. Cell. 2006; 125(1):33–45. https://doi.org/10.1016/j.cell.2006.03.002 PMID: 16615888.
4. Matsui T, Bessho Y. Left-right asymmetry in zebrafish. Cellular and molecular life sciences: CMLS. 2012; 69(18):3069–77. https://doi.org/10.1007/s00018-012-0985-6 PMID: 22527718.
5. Maclean K, Dunwoodie SL. Breaking symmetry: a clinical overview of left-right patterning. Clinical genetics. 2004; 65(6):441–57. https://doi.org/10.1111/j.0009-9163.2004.00258.x PMID: 15151499.
6. Ramsdell AF. Left-right asymmetry and congenital cardiac defects: getting to the heart of the matter in vertebrate left-right axis determination. Developmental biology. 2005; 288(1):1–20. https://doi.org/10.1016/j.ydbio.2005.07.038 PMID: 16289136.
7. Sherr CJ, Roberts JM. CDK inhibitors: positive and negative regulators of G1-phase progression. Genes & development. 1999; 13(12):1501–12. https://doi.org/10.1101/gad.13.12.1501 PMID: 10385618.
8. Dalton S. Linking the Cell Cycle to Cell Fate Decisions. Trends in cell biology. 2015; 25(10):592–600. https://doi.org/10.1016/j.tcb.2015.07.007 PMID: 26410405
9. Dalton S. G1 compartmentalization and cell fate coordination. Cell. 2013; 155(1):13–4. https://doi.org/10.1016/j.cell.2013.09.015 PMID: 24074854.
10. Julian LM, Carpenedo RL, Rothberg JL, Stanford WL. Formula G1: Cell cycle in the driver's seat of stem cell fate determination. BioEssays: news and reviews in molecular, cellular and developmental biology. 2016; 38(4):325–32. https://doi.org/10.1002/bies.201500187 PMID: 26857166.
11. Pauklin S, Vallier L. The cell-cycle state of stem cells determines cell fate propensity. Cell. 2013; 155(1):135–47. https://doi.org/10.1016/j.cell.2013.08.031 PMID: 24074866
12. Liu L, Michowski W, Inuzuka H, Shimizu K, Nihira NT, Chick JM, et al. G1 cyclins link proliferation, pluripotency and differentiation of embryonic stem cells. Nature cell biology. 2017; 19(3):177–88. https://doi.org/10.1038/ncb3474 PMID: 28192421
13. Lange C, Huttner WB, Calegari F. Cdk4/cyclinD1 overexpression in neural stem cells shortens G1, delays neurogenesis, and promotes the generation and expansion of basal progenitors. Cell stem cell. 2009; 5(3):320–31. https://doi.org/10.1016/j.stem.2009.05.026 PMID: 19733543.
14. Cooper MS, D'Amico LA. A cluster of noninvoluting endocytic cells at the margin of the zebrafish blastoderm marks the site of embryonic shield formation. Developmental biology. 1996; 180(1):184–98. https://doi.org/10.1006/dbio.1996.0294 PMID: 8948584.
15. Oteiza P, Koppen M, Concha ML, Heisenberg CP. Origin and shaping of the laterality organ in zebrafish. Development. 2008; 135(16):2807–13. https://doi.org/10.1242/dev.022228 PMID: 18635607.
16. Gokey JJ, Dasgupta A, Amack JD. The V-ATPase accessory protein Atp6ap1b mediates dorsal forerunner cell proliferation and left-right asymmetry in zebrafish. Developmental biology. 2015; 407(1):115–30. https://doi.org/10.1016/j.ydbio.2015.08.002 PMID: 26254189
17. Caron A, Xu X, Lin X. Wnt/beta-catenin signaling directly regulates Foxj1 expression and ciliogenesis in zebrafish Kupffer's vesicle. Development. 2012; 139(3):514–24. https://doi.org/10.1242/dev.071746 PMID: 22190638
18. Zhang M, Zhang J, Lin SC, Meng A. beta-Catenin 1 and beta-catenin 2 play similar and distinct roles in left-right asymmetric development of zebrafish embryos. Development. 2012; 139(11):2009–19. https://doi.org/10.1242/dev.074435 PMID: 22535411.
19. Brody SL, Yan XH, Wuerffel MK, Song SK, Shapiro SD. Ciliogenesis and left-right axis defects in forkhead factor HFH-4-null mice. American journal of respiratory cell and molecular biology. 2000; 23(1):45–51. https://doi.org/10.1165/ajrcmb.23.1.4070 PMID: 10873152.
20. Chen J, Knowles HJ, Hebert JL, Hackett BP. Mutation of the mouse hepatocyte nuclear factor/forkhead homologue 4 gene results in an absence of cilia and random left-right asymmetry. The Journal of clinical investigation. 1998; 102(6):1077–82. https://doi.org/10.1172/JCI4786 PMID: 9739041

21. Yu X, Ng CP, Habacher H, Roy S. Foxj1 transcription factors are master regulators of the motile ciliogenic program. Nature genetics. 2008; 40(12):1445–53. https://doi.org/10.1038/ng.263 PMID: 19011630.

22. Stubbs JL, Oishi I, Izpisua Belmonte JC, Kintner C. The forkhead protein Foxj1 specifies node-like cilia in Xenopus and zebrafish embryos. Nature genetics. 2008; 40(12):1454–60. https://doi.org/10.1038/ng.267 PMID: 19011629

23. Neugebauer JM, Amack JD, Peterson AG, Bisgrove BW, Yost HJ. FGF signalling during embryo development regulates cilia length in diverse epithelia. Nature. 2009; 458(7238):651–4. https://doi.org/10.1038/nature07753 PMID: 19242413

24. Kim MJ, Rhee M, Ro H. Lnx2b, an E3 ubiquitin ligase, in dorsal forerunner cells and Kupffer's vesicle is required for specification of zebrafish left-right laterality. Anim Cells Syst. 2014; 18(5):333–9. https://doi.org/10.1080/19768354.2014.968205

25. Raz E, Mahabaleshwar H. Chemokine signaling in embryonic cell migration: a fisheye view. Development. 2009; 136(8):1223–9. https://doi.org/10.1242/dev.022418 PMID: 19304885.

26. Boldajipour B, Doitsidou M, Tarbashevich K, Laguri C, Yu SR, Ries J, et al. Cxcl12 evolution—subfunctionalization of a ligand through altered interaction with the chemokine receptor. Development. 2011; 138(14):2909–14. https://doi.org/10.1242/dev.068379 PMID: 21693511.

27. Peled A, Petit I, Kollet O, Magid M, Ponomaryov T, Byk T, et al. Dependence of human stem cell engraftment and repopulation of NOD/SCID mice on CXCR4. Science. 1999; 283(5403):845–8. https://doi.org/10.1126/science.283.5403.845 PMID: 9933168.

28. Doitsidou M, Reichman-Fried M, Stebler J, Koprunner M, Dorries J, Meyer D, et al. Guidance of primordial germ cell migration by the chemokine SDF-1. Cell. 2002; 111(5):647–59. https://doi.org/10.1016/s0092-8674(02)01135-2 PMID: 12464177.

29. David NB, Sapede D, Saint-Etienne L, Thisse C, Thisse B, Dambly-Chaudiere C, et al. Molecular basis of cell migration in the fish lateral line: role of the chemokine receptor CXCR4 and of its ligand, SDF1. Proceedings of the National Academy of Sciences of the United States of America. 2002; 99 (25):16297–302. https://doi.org/10.1073/pnas.252339399 PMID: 12444253

30. Knaut H, Werz C, Geisler R, Nusslein-Volhard C, Tubingen Screen C. A zebrafish homologue of the chemokine receptor Cxcr4 is a germ-cell guidance receptor. Nature. 2003; 421(6920):279–82. https://doi.org/10.1038/nature01338 PMID: 12508118.

31. Nair S, Schilling TF. Chemokine signaling controls endodermal migration during zebrafish gastrulation. Science. 2008; 322(5898):89–92. https://doi.org/10.1126/science.1160038 PMID: 18719251

32. Olesnicky Killian EC, Birkholz DA, Artinger KB. A role for chemokine signaling in neural crest cell migration and craniofacial development. Developmental biology. 2009; 333(1):161–72. https://doi.org/10.1016/j.ydbio.2009.06.031 PMID: 19576198

33. Li L, Mao A, Wang P, Ning G, Cao Y, Wang Q. Endodermal pouch-expressed dmrt2b is important for pharyngeal cartilage formation. Biology open. 2018; 7(12): bio035444. https://doi.org/10.1242/bio.035444 PMID: 30341107

34. Siekmann AF, Standley C, Fogarty KE, Wolfe SA, Lawson ND. Chemokine signaling guides regional patterning of the first embryonic artery. Genes & development. 2009; 23(19):2272–7. https://doi.org/10.1101/gad.1813509 PMID: 19797767

35. Chong SW, Emelyanov A, Gong Z, Korzh V. Expression pattern of two zebrafish genes, cxcr4a and cxcr4b. Mechanisms of development. 2001; 109(2):347–54. PMID: 11731248.

36. Roussigne M, Bianco IH, Wilson SW, Blader P. Nodal signalling imposes left-right asymmetry upon neurogenesis in the habenular nuclei. Development. 2009; 136(9):1549–57. https://doi.org/10.1242/dev.034793 PMID: 19363156

37. Amack JD, Yost HJ. The T box transcription factor no tail in ciliated cells controls zebrafish left-right asymmetry. Current biology: CB. 2004; 14(8):685–90. https://doi.org/10.1016/j.cub.2004.04.002 PMID: 15084283.

38. Bussmann J, Wolfe SA, Siekmann AF. Arterial-venous network formation during brain vascularization involves hemodynamic regulation of chemokine signaling. Development. 2011; 138(9):1717–26. https://doi.org/10.1242/dev.059881 PMID: 21429983

39. Hamada H, Meno C, Watanabe D, Saijoh Y. Establishment of vertebrate left-right asymmetry. Nature reviews Genetics. 2002; 3(2):103–13. https://doi.org/10.1038/nrg732 PMID: 11836504.

40. Aw S, Levin M. Is left-right asymmetry a form of planar cell polarity? Development. 2009; 136(3):355–66. https://doi.org/10.1242/dev.015974 PMID: 19141667

41. Sugiyama M, Sakaue-Sawano A, Iimura T, Fukami K, Kitaguchi T, Kawakami K, et al. Illuminating cell-cycle progression in the developing zebrafish embryo. Proceedings of the National Academy of

Sciences of the United States of America. 2009; 106(49):20812–7. https://doi.org/10.1073/pnas.0906464106 PMID: 19923430

42. Klein S, Abraham M, Bulvik B, Dery E, Weiss ID, Barashi N, et al. CXCR4 Promotes Neuroblastoma Growth and Therapeutic Resistance through miR-15a/16-1-Mediated ERK and BCL2/Cyclin D1 Pathways. Cancer research. 2018; 78(6):1471–83. https://doi.org/10.1158/0008-5472.CAN-17-0454 PMID: 29259008.

43. Mo W, Chen J, Patel A, Zhang L, Chau V, Li Y, et al. CXCR4/CXCL12 mediate autocrine cell- cycle progression in NF1-associated malignant peripheral nerve sheath tumors. Cell. 2013; 152(5):1077–90. https://doi.org/10.1016/j.cell.2013.01.053 PMID: 23434321

44. Wang Y, Xu P, Qiu L, Zhang M, Huang Y, Zheng JC. CXCR7 Participates in CXCL12-mediated Cell Cycle and Proliferation Regulation in Mouse Neural Progenitor Cells. Current molecular medicine. 2016; 16(8):738–46. https://doi.org/10.2174/1566524016666160829153453 PMID: 27573194

45. Bolcome RE 3rd, Chan J. Constitutive MEK1 activation rescues anthrax lethal toxin-induced vascular effects in vivo. Infection and immunity. 2010; 78(12):5043–53. https://doi.org/10.1128/IAI.00604-10 PMID: 20855511

46. Sherr CJ. D-type cyclins. Trends in biochemical sciences. 1995; 20(5):187–90. PMID: 7610482.

47. Fry DW, Harvey PJ, Keller PR, Elliott WL, Meade M, Trachet E, et al. Specific inhibition of cyclin-dependent kinase 4/6 by PD 0332991 and associated antitumor activity in human tumor xenografts. Molecular cancer therapeutics. 2004; 3(11):1427–38. PMID: 15542782.

48. De Azevedo WF, Leclerc S, Meijer L, Havlicek L, Strnad M, Kim SH. Inhibition of cyclin-dependent kinases by purine analogues: crystal structure of human cdk2 complexed with roscovitine. European journal of biochemistry. 1997; 243(1–2):518–26. https://doi.org/10.1111/j.1432-1033.1997.0518a.x PMID: 9030780.

49. Matsushime H, Ewen ME, Strom DK, Kato JY, Hanks SK, Roussel MF, et al. Identification and properties of an atypical catalytic subunit (p34PSK-J3/cdk4) for mammalian D type G1 cyclins. Cell. 1992; 71 (2):323–34. https://doi.org/10.1016/0092-8674(92)90360-o PMID: 1423597.

50. Songyang Z, Blechner S, Hoagland N, Hoekstra MF, Piwnica-Worms H, Cantley LC. Use of an oriented peptide library to determine the optimal substrates of protein kinases. Current biology: CB. 1994; 4 (11):973–82. https://doi.org/10.1016/s0960-9822(00)00221-9 PMID: 7874496.

51. Ciechanover A, Stanhill A. The complexity of recognition of ubiquitinated substrates by the 26S proteasome. Biochimica et biophysica acta. 2014; 1843(1):86–96. https://doi.org/10.1016/j.bbamcr.2013.07.007 PMID: 23872423.

52. Johnson BM, DeBose-Boyd RA. Underlying mechanisms for sterol-induced ubiquitination and ER-associated degradation of HMG CoA reductase. Seminars in cell & developmental biology. 2018; 81:121–8. https://doi.org/10.1016/j.semcdb.2017.10.019 PMID: 29107682.

53. Finley D, Sadis S, Monia BP, Boucher P, Ecker DJ, Crooke ST, et al. Inhibition of proteolysis and cell cycle progression in a multiubiquitination-deficient yeast mutant. Molecular and cellular biology. 1994; 14(8):5501–9. https://doi.org/10.1128/mcb.14.8.5501 PMID: 8035826

54. Ju D, Xie Y. Proteasomal degradation of RPN4 via two distinct mechanisms, ubiquitin-dependent and -independent. The Journal of biological chemistry. 2004; 279(23):23851–4. https://doi.org/10.1074/jbc.C400111200 PMID: 15090546.

55. Liu C, Li Y, Semenov M, Han C, Baeg GH, Tan Y, et al. Control of beta-catenin phosphorylation/degradation by a dual-kinase mechanism. Cell. 2002; 108(6):837–47. https://doi.org/10.1016/s0092-8674(02)00685-2 PMID: 11955436.

56. Sanchez-Lanzas R, Castano JG. Proteins directly interacting with mammalian 20S proteasomal subunits and ubiquitin-independent proteasomal degradation. Biomolecules. 2014; 4(4):1140–54. https://doi.org/10.3390/biom4041140 PMID: 25534281

57. Hiyama H, Yokoi M, Masutani C, Sugasawa K, Maekawa T, Tanaka K, et al. Interaction of hHR23 with S5a. The ubiquitin-like domain of hHR23 mediates interaction with S5a subunit of 26 S proteasome. The Journal of biological chemistry. 1999; 274(39):28019–25. https://doi.org/10.1074/jbc.274.39.28019 PMID: 10488153.

58. Sakata E, Yamaguchi Y, Kurimoto E, Kikuchi J, Yokoyama S, Yamada S, et al. Parkin binds the Rpn10 subunit of 26S proteasomes through its ubiquitin-like domain. EMBO reports. 2003; 4(3):301–6. https://doi.org/10.1038/sj.embor.embor764 PMID: 12634850

59. Du J, Zhang J, He T, Li Y, Su Y, Tie F, et al. Stuxnet Facilitates the Degradation of Polycomb Protein during Development. Developmental cell. 2016; 37(6):507–19. https://doi.org/10.1016/j.devcel.2016.05.013 PMID: 27326929.

60. Golson ML, Kaestner KH. Fox transcription factors: from development to disease. Development. 2016; 143(24):4558–70. https://doi.org/10.1242/dev.112672 PMID: 27965437

61. Stroud JC, Wu YQ, Bates DL, Han AD, Nowick K, Paabo S, et al. Structure of the forkhead domain of FOXP2 bound to DNA. Structure. 2006; 14(1):159–66. https://doi.org/10.1016/j.str.2005.10.005 PMID: 16407075

62. Ford MJ, Yeyati PL, Mali GR, Keighren MA, Waddell SH, Mjoseng HK, et al. A Cell/Cilia Cycle Biosensor for Single-Cell Kinetics Reveals Persistence of Cilia after G1/S Transition Is a General Property in Cells and Mice. Developmental cell. 2018; 47(4):509–23 e5. https://doi.org/10.1016/j.devcel.2018.10.027 PMID: 30458140

63. Komatsu Y, Kaartinen V, Mishina Y. Cell cycle arrest in node cells governs ciliogenesis at the node to break left-right symmetry. Development. 2011; 138(18):3915–20. https://doi.org/10.1242/dev.068833 PMID: 21831921

64. Noel ES, Verhoeven M, Lagendijk AK, Tessadori F, Smith K, Choorapoikayil S, et al. A Nodal-independent and tissue-intrinsic mechanism controls heart-looping chirality. Nature communications. 2013; 4:2754. https://doi.org/10.1038/ncomms3754 PMID: 24212328

65. Anders L, Ke N, Hydbring P, Choi YJ, Widlund HR, Chick JM, et al. A systematic screen for CDK4/6 substrates links FOXM1 phosphorylation to senescence suppression in cancer cells. Cancer cell. 2011; 20(5):620–34. https://doi.org/10.1016/j.ccr.2011.10.001 PMID: 22094256

66. Huang H, Regan KM, Lou Z, Chen J, Tindall DJ. CDK2-dependent phosphorylation of FOXO1 as an apoptotic response to DNA damage. Science. 2006; 314(5797):294–7. https://doi.org/10.1126/science.1130512 PMID: 17038621.

67. Rane SG, Dubus P, Mettus RV, Galbreath EJ, Boden G, Reddy EP, et al. Loss of Cdk4 expression causes insulin-deficient diabetes and Cdk4 activation results in beta-islet cell hyperplasia. Nature genetics. 1999; 22(1):44–52. https://doi.org/10.1038/8751 PMID: 10319860

68. Malumbres M, Sotillo R, Santamaria D, Galan J, Cerezo A, Ortega S, et al. Mammalian cells cycle without the D-type cyclin-elependent kinases Cdk4 and Cdk6. Cell. 2004; 118(4):493–504. https://doi.org/10.1016/j.cell.2004.08.002 PMID: 15315761

69. Berthet C, Aleem E, Coppola V, Tessarollo L, Kaldis P. Cdk2 knockout mice are viable. Current Biology. 2003; 13(20):1775–85. https://doi.org/10.1016/j.cub.2003.09.024 PMID: 14561402

70. Berthet C, Klarmann KD, Hilton MB, Suh HC, Keller JR, Kiyokawa H, et al. Combined loss of Cdk2 and Cdk4 results in embryonic lethality and Rb hypophosphorylation. Developmental cell. 2006; 10(5):563–73. https://doi.org/10.1016/j.devcel.2006.03.004 PMID: 16678773

71. Erales J, Coffino P. Ubiquitin-independent proteasomal degradation. Biochimica et biophysica acta. 2014; 1843(1):216–21. https://doi.org/10.1016/j.bbamcr.2013.05.008 PMID: 23684952

72. Hwang J, Winkler L, Kalejta RF. Ubiquitin-independent proteasomal degradation during oncogenic viral infections. Biochimica et biophysica acta. 2011; 1816(2):147–57. https://doi.org/10.1016/j.bbcan.2011.05.005 PMID: 21664948

73. Cota CD, Bagher P, Pelc P, Smith CO, Bodner CR, Gunn TM. Mice with mutations in Mahogunin ring finger-1 (Mgrn1) exhibit abnormal patterning of the left-right axis. Developmental dynamics: an official publication of the American Association of Anatomists. 2006; 235(12):3438–47. https://doi.org/10.1002/dvdy.20992 PMID: 17075880.

74. Yoshiba S, Hamada H. Roles of cilia, fluid flow, and Ca2+ signaling in breaking of left-right symmetry. Trends in genetics: TIG. 2014; 30(1):10–7. https://doi.org/10.1016/j.tig.2013.09.001 PMID: 24091059.

75. Abdi K, Lai CH, Paez-Gonzalez P, Lay M, Pyun J, Kuo CT. Uncovering inherent cellular plasticity of multiciliated ependyma leading to ventricular wall transformation and hydrocephalus. Nature communications. 2018; 9(1):1655. https://doi.org/10.1038/s41467-018-03812-w PMID: 29695808

76. Hsieh LS, Su WM, Han GS, Carman GM. Phosphorylation regulates the ubiquitin-independent degradation of yeast Pah1 phosphatidate phosphatase by the 20S proteasome. The Journal of biological chemistry. 2015; 290(18):11467–78. https://doi.org/10.1074/jbc.M115.648659 PMID: 25809482

77. Ning G, Liu X, Dai M, Meng A, Wang Q. MicroRNA-92a upholds Bmp signaling by targeting noggin3 during pharyngeal cartilage formation. Developmental cell. 2013; 24(3):283–95. https://doi.org/10.1016/j.devcel.2012.12.016 PMID: 23410941.